Photosensitized Reactions of a Phenolic Carbonyl from Wood Combustion in the Aqueous Phase – Chemical Evolution and Light Absorption Properties of AqSOA

Wenqing Jiang[1,2], Maria V Misovich[3], Anusha P.S. Hettiyadura[3], Alexander Laskin[3,4], Alexander S. McFall[2,5], Cort Anastasio[2,5], Qi Zhang[1,2]*

[1]Department of Environmental Toxicology, University of California, Davis, CA

[2]Agricultural and Environmental Chemistry Graduate Group, University of California, Davis, CA

[3]Department of Chemistry, Purdue University, West Lafayette, IN

[4]Department of Earth, Atmospheric and Planetary Sciences, Purdue University, West Lafayette, IN

[5]Department of Land, Air, and Water Resources, University of California, Davis, CA

*Corresponding author: Qi Zhang

Email: dkwzhang@ucdavis.edu

Phone: 530-752-5779

Abstract

Guaiacyl acetone (GA) is a phenolic carbonyl emitted in significant quantities by wood combustion that undergoes rapid aqueous-phase oxidation to produce aqueous secondary organic aerosol (aqSOA). We investigate the photosensitized oxidation of GA by an organic triplet excited state ($^3C^*$) and the formation and aging of the resulting aqSOA in wood smoke-influenced fog/cloud water. The chemical transformations of the aqSOA were characterized in situ using a high-resolution time-of-flight aerosol mass spectrometer. Additionally, aqSOA samples collected over different time periods were analyzed using high-performance liquid chromatography coupled with a photodiode array detector and a high-resolution Orbitrap mass spectrometer (HPLC-PDA-HRMS) to provide details on the molecular composition and optical properties of brown carbon (BrC) chromophores. Our results show efficient formation of aqSOA from GA, with an average mass yield around 80%. The composition and BrC properties of the aqSOA changed significantly over the course of reaction. Three generations of aqSOA products were identified via Positive Matrix Factorization analysis of the AMS data. Oligomerization and functionalization dominated the production of the first-generation aqSOA, whereas fragmentation and ring-opening reactions controlled the formation of more oxidized second- and third-generation products. Significant formation of BrC was observed in the early stages of the photoreaction, while organic acids were produced throughout the experiment. High-molecular-weight molecules ($m/z > 180$) with high aromaticity were identified via HPLC-PDA-HRMS and were found to account for a majority of the UV-vis absorption of the aqSOA.

Keywords

Phenolic Carbonyls, Aqueous Secondary Organic Aerosol, Brown Carbon

Synopsis

This work characterizes the aqSOA and BrC formation from a phenolic carbonyl emitted from biomass burning, and helps to improve our understanding of the evolution of emissions from biomass burning.

Graphic for Table of Contents (TOC)/Abstract Art

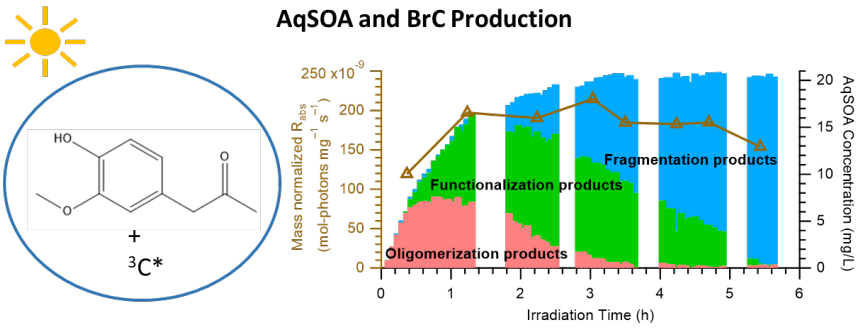

1. Introduction

Biomass burning (BB) emissions – from residential stoves and fireplaces, wildland fires and prescribed agricultural burns – are a major source of particulate matter (PM) in the atmosphere, contributing approximately 10–50% of the total organic aerosol (OA) mass.[1,2] Aerosols from BB sources have significant impacts on climate, air quality, and human health.[3–8] Emissions from residential wood burning are frequently a major contributor to fine PM pollution in urban regions in winter.[9–15] Wildfires, a major natural hazard, have been reported to emit more PM than anthropogenic sources in many parts of the world.[6,16,17] BB aerosols contribute significantly to global warming due to their light-absorbing properties.[18,19] Previous studies have reported that brown carbon (BrC) chromophores observed in BB aerosols include lignin pyrolysis products, distillation products (coumarins and flavonoids), nitroaromatics, and polycyclic aromatic hydrocarbons (PAHs).[20] In addition, exposure to wood smoke particles cause health problems such as acute respiratory infections, tuberculosis, lung cancer, and cataracts.[21]

BB smoke consists of complex mixtures of particles and gases. Oxidation of volatile organic compounds (VOCs) emitted from BB is an important source of secondary organic aerosol (SOA) in the atmosphere.[22–26] During the photooxidation of BB emissions, both chromophore formation and sunlight bleaching can occur, leading to changes of aerosols optical properties.[27–30] Previous studies have reported that aqueous-phase photo-oxidation of BB emissions can increase the absorbance of BrC through the formation of aromatic dimer compounds and functionalized products.[29] On the other hand, longer aging generally leads to photobleaching of the BrC in BB

emissions, which can be mainly attributed to decomposition of chromophoric aromatics, nitrogen-containing organics, and high-molecular weight components.[31] Also, the wavelength dependence of BrC absorption generally increases with prolonged aging.[28]

Phenols are emitted from BB in significant quantities through lignin pyrolysis. Aldehyde- and ketone-functionalized phenols (i.e., phenolic carbonyls) account for 18% and 22% of total phenol emissions from the burning of hardwood and softwood, respectively.[32,33] Most of the phenolic carbonyls emitted from BB are of intermediate volatility and have high Henry's law constants.[34,35] They readily partition into atmospheric aqueous phases (e.g., deliquesced aerosol, cloud and fog droplets), where reactions can occur to form low-volatility materials which remain in the particle phase upon water evaporation, yielding aqSOA.[35] Conjugated phenolic carbonyls, i.e., phenols with the carbonyl groups directly connected to the aromatic ring, tend to have high solar absorbance and a propensity to form aqSOA and brown carbon (BrC) through direct photochemical reactions at fast rates.[35–38]

Guaiacyl acetone (GA; 4-Hydroxy-3-methoxyphenylacetone; $C_{10}H_{12}O_3$) is a phenolic carbonyl released from BB with emission rates of 12 - 41 μg g_{fuel}^{-1}. This compound was detected in the atmosphere in the range of 0.3 - 0.6 ng m^{-3},[39] which is comparable to the concentrations of the most common phenols (e.g., guaiacol and syringol). The high Henry's law constant of GA (1.2×10^6 M atm^{-1})[34] suggests that aqueous reactions are an important atmospheric sink for this molecule in cloud/fog conditions. For example, within a cloud/fog with a liquid water content of 0.3 g-H_2O m^{-3}, ~ 90% of GA is estimated to present in the aqueous phase at Henry's law equilibrium. Additionally, since the replenishment of the aqueous-phase GA by partitioning from the gas phase is very fast (time scale of minutes) compared to aqueous reaction (time scale of hours),[40] aqueous reactions are likely major pathways for GA transformation under cloudy or foggy conditions. Compared with conjugated phenolic carbonyls, such as vanillin, acetovanillone, acetosyringone and syringaldehyde, GA absorbs little sunlight and therefore is more resilient to direct photodegradation.[35] Aqueous-phase aging of GA may occur through oxidation by hydroxyl radical (•OH), triplet excited states of carbon ($^3C^*$), and singlet molecular oxygen ($^1O_2^*$). $^3C^*$ is a particularly important oxidant for phenols as the reactions usually generate aqSOA at faster rates and higher mass yields compared to OH oxidation of phenols.[35,41–46] Furthermore, there is evidence [46,47] that $^3C^*$ oxidation of phenols produces light-absorbing oligomers and high molecular weight derivatives more efficiently compared to OH oxidation or direct photodegradation.

One important source of atmospheric $^3C^*$ is light-absorbing organic compounds emitted from BB.[48] Sunlight absorption by the organics can promote the ground states of chromophores to the triplet excited states in the aqueous phase.[35,41,42] Significant formation of $^3C^*$ has been observed in fog droplets and particle-bound water under solar irradiation [49,50] and the reactions of phenols with $^3C^*$ have been shown to be an effective formation pathway for highly oxidized aqSOA with average oxygen-to-carbon ratio close to 1.[35,42,45–47]

In this study, we investigate the photochemical formation and aging of aqSOA through the aqueous reactions of GA with $^3C^*$ under solar irradiation in wood smoke-influenced fog and cloud waters. We perform aqueous-phase photoreaction experiments of GA in the presence of $^3C^*$, characterize the chemical composition and light absorption properties of the formed aqSOA and examine the formation pathways, molecular composition, and optical properties of the BrC chromophores within the aqSOA. Although many studies on the photo-oxidation of biomass burning emissions have been done previously, this study uses GA as a model compound to investigate the aqueous photosensitized reactions of phenolic carbonyls and their potential to produce aqSOA and BrC, which have not been thoroughly investigated before.

2. Experimental Methods

2.1 Aqueous-phase Photochemical Reaction

Experimental solutions were prepared with 100 μM (18 mg/L) of GA and 5 μM (0.83 mg/L) of 3,4-DMB (3,4-dimethoxybenzaldehyde; $C_9H_{10}O_3$) as a source of $^3C^*$, with the pH adjusted to 4.6 using sulfuric acid to mimic the wood burning-impacted cloud and fog waters.[41,50–52] In addition, 10 mg/L of ammonium sulfate was added into the solution as an internal standard for quantification of SOA mass concentration using a high-resolution time-of-flight aerosol mass spectrometer (HR-TOF-AMS; Aerodyne Res. Inc.).[45] The prepared solution was placed in 110 mL Pyrex tubes, continuously magnetically stirred, and illuminated with simulated sunlight inside an RPR-200 photoreactor system described elsewhere [53] (Fig. S1). Note that for $^3C^*$ exposure, the rate of light absorption was ~7 times faster in our Photoreactor System than that in the midday winter solstice sunlight in Davis. A dark control sample was prepared in the same manner, wrapped with aluminum foil, and placed inside the photoreactor during the illumination experiment.

2.2 Sample Analyses

Throughout the course of each experiment, a Shimadzu LC-10AD HPLC pump was used to draw solution at a constant flow rate (1.0 mL/min) alternatively from the illuminated and the dark control tubes. The solution was delivered to a constant output atomizer and atomized continuously in purified pressurized air. The resulting particles were dried to RH < 5% using a diffusion dryer and analyzed by AMS in real-time. The excess solution dripping from the atomizer was collected at different time intervals over the course of each experiment and the aliquots were stored frozen (-20 °C) for offline analysis of: 1) GA and 3,4-DMB concentrations using HPLC-PDA (Agilent Technologies Inc.);[34] 2) concentrations of organic anions, including formate, acetate, malate, malonate, and oxalate, using a Metrohm anion ion chromatograph (IC);[54] 3) UV-visible absorption using a Shimadzu UV-2501PC spectrophotometer; and 4) molecular composition and optical properties of aqSOA chromophores using HPLC-PDA-HRMS.[55]

2.2.1 Real-time AMS Analysis of aqSOA Bulk Composition and Yield Calculation

Real-time changes in the mass concentration and bulk chemical composition of the aqSOA were measured by an AMS operated alternatively between "V" and "W" modes (mass resolution (m/Δm) of ~3000 and ~5000, respectively) to acquire mass spectra up to 485 and 280 amu, respectively. The data was processed using the standard AMS data analysis toolkits (SQUIRREL v1.56D and PIKA 1.15D). According to our previous studies, we assume the particles are effectively dried by the diffusion drier, which led to RH < 5% at the AMS inlet, and the contribution of particle water in the AMS mass spectra was negligible.[46] The organic H_2O^+ signal (org-H_2O^+ hereafter) was thus determined as the difference between the measured H_2O^+ signal and the sulfate-associated H_2O^+ signal. The derived org-H_2O^+ signal was somewhat noisy, but it showed a good correlation ($r^2 = 0.66$) with the measured organic CO_2^+ signal with a slope of 0.4 (Fig. S2). To reduce noise in the calculated elemental ratios, we thus parameterized the org-H_2O^+ related signals of aqSOA according to the measured CO_2^+ signal, i.e., org-$H_2O^+ = 0.4 \times CO_2^+$, org-$OH^+ = 0.25 \times$ org-H_2O^+ and org-$O^+ = 0.04 \times$ org-H_2O^+.[46,56] The atomic oxygen-to-carbon (O/C) ratio, hydrogen-to-carbon (H/C) ratio, and organic mass-to-organic-carbon (OM/OC) ratio were

subsequently determined. The average oxidation state of carbon (OS_C) in aqSOA is determined as $OS_C = 2\ O/C - H/C$,[57] since the aqSOA studied here mainly consisted of C, H, and O atoms with a negligible contribution from peroxide groups.[58]

The aqSOA mass yield was calculated using Equation 1:

$$\text{SOA yield} = \frac{[Org]_t - [Org]_0}{[GA]_0 - [GA]_t} = \frac{[Org_{AMS}]_t \times \frac{[AS]_t}{[AS_{AMS}]_t} - [Org_{AMS}]_0 \times \frac{[AS]_0}{[AS_{AMS}]_0}}{[GA]_0 - [GA]_t} \quad (1)$$

where [Org], [AS], and [GA] denote the aqSOA, sulfate and GA concentrations (mg L^{-1}) in the solution, respectively. The $[Org_{AMS}]$ and $[AS_{AMS}]$ denote the apparent concentrations (μg m^{-3}) of aqSOA and sulfate measured by AMS. The subscripts indicate irradiation time, e.g., $[GA]_0$ is the initial concentration of GA. Here, the concentration of sulfate in the solution is assumed to be constant during irradiation (i.e., $[AS]_t = [AS]_0$).

Positive matrix factorization (PMF) analysis was performed to investigate the chemical evolution of the aqSOA. The input data were the organic mass spectral matrix and the corresponding error matrix generated within PIKA. The PMF results were evaluated using the PMF Evaluation Toolkit (PET v3.05 downloaded from: http://cires1.colorado.edu/jimenez-group/wiki/index.php/PMF-AMS_Analysis_Guide).[59] A four-factor solution was chosen based on the evaluation criteria outlined in Zhang et al..[60] A summary of the diagnostic plots for the 4-factor PMF solution is presented in Fig. S3. Selecting fewer or more factors leads to either high residuals or splitting of the factors. Among the four resolved factors, three are representative of different generations of aqSOA and the fourth is a background factor likely due to chemical impurities present in the reagents. The time series and mass spectrum of the background factor are shown in Fig. S4. The mass spectrum of the background factor looks very different than the spectra of the aqSOA factors and its concentration remained nearly constant throughout the experiment. This factor only accounts for a minor fraction of the organic aerosol mass measured by AMS (3%), and therefore likely has a negligible effect on the bulk composition of the aqSOA.

2.2.2 Offline UV-vis Absorption Measurements

The light absorption coefficient (α_λ, cm^{-1}) of the solution was calculated using Equation 2:

$$\alpha_\lambda = \frac{A_\lambda}{l} \quad (2)$$

where A_λ is the base-10 light absorbance of the aqSOA solution at wavelength λ (i.e., A_λ = total measured absorbance at λ – the absorbance contributed by GA and 3,4-DMB at λ) and l is the pathlength of the cuvette (cm).

The mass absorption coefficient for the aqSOA (MAC_λ, $cm^2\ g^{-1}$) was then calculated as:

$$MAC_\lambda = \frac{2.303\ \alpha_\lambda}{C} \times 10^{-6} \quad (3)$$

where C is the aqSOA mass concentration in $mg\ L^{-1}$, and 2.303 is a base conversion factor between lg and ln. The carbon-based MAC_λ, $cm^2\ g\text{-}C^{-1}$, can be derived by multiplying MAC_λ by the OM/OC ratio of the aqSOA.

Additionally, the rate of sunlight absorption (R_{abs}, mol-photons $L^{-1}\ s^{-1}$) of the aqSOA solution was calculated using:

$$R_{abs} = 2.303 \times 10^3 \times N_A \times \int_{300nm}^{700nm} \alpha_\lambda \times I_\lambda \times d\lambda \quad (4)$$

where 2.303 is a base conversion, 10^3 is a units conversion factor ($cm^3\ L^{-1}$), N_A is Avogadro's number, I_λ is the winter-solstice actinic flux (photons $cm^{-2}\ s^{-1}\ nm^{-1}$) in Davis, CA, calculated using the Tropospheric Ultraviolet and Visible (TUV) Radiation Model (http://cprm.acom.ucar.edu/Models/TUV/Interactive_TUV/), and $d\lambda$ is the interval between adjacent wavelengths in the TUV output (2 nm).

2.2.3 HPLC-PDA-HRMS analysis of BrC in aqSOA

The aqSOA samples were analyzed using an HPLC system coupled with a PDA detector (Vanquish™, Thermo Scientific Inc) and a high resolution Orbitrap mass spectrometer, Q Exactive™ HF-X (Thermo Scientific Inc) to identify and characterize BrC chromophores. LC-MS grade water was used as a blank. All solvents, including mobile phases, were Optima™ LC/MS grade, purchased from Fisher Chemical. The HPLC separation was performed according to Lin et al., 2018.[55] Briefly, organic compounds were separated on a reversed-phase column (Luna® C18(2), 150 × 2 mm, 5 μm particles, 100 Å pores; Phenomenex Inc.) using water with 0.1% (v/v) formic acid (A) and acetonitrile with 0.1% (v/v) formic acid (B) as mobile phases at a flow rate of 0.200 mL min^{-1}, 0-3 min at 10% B, 3-63 min a linear increase to 90% B; 63-75 min hold at 90% B, 75-90 min a linear gradient to 100% B, 90-100 hold at 100% B, 100-101 min a linear decrease

to 10% B, 101-120 min equilibration at 10% B to prepare for the next run. A sample injection volume of 15 μL was used. Light absorption between 250 – 680 nm was recorded by the PDA detector. The HPLC separated organic compounds were ionized using an electrospray ionization (ESI) source operated in alternating positive and negative ion modes. This study reports the data acquired in negative mode. The analysis was performed in the full scan mode in the mass range m/z 80 – 1200 at a mass resolution of 24,000 at 200 m/z. A spray voltage of 2.5 kV was used in the negative ion mode. A capillary temperature of 250 ˚C was used. A sheath gas flow rate of 30 arbitrary units (arb), auxillary gas flow rate of 10 arb and a sweep gas flow rate of 1 arb were used. The mass calibration was performed using Thermo Scientific™ Pierce™ negative ion calibration solution (PI-88324). The highly polar CHO components of aqSOA were mostly observed as deprotonated ions $[M\text{-}H]^-$, while some of them were also observed as cluster ions with sodium formate $[M+(HCOONa)_x\text{-}H]^-$. Xcalibur (Thermo Scientific) was used to acquire raw data. MZmine 2.39 (http://mzmine.github.io/) software was used to select peaks.[61] Peaks that occurred in the blank sample were subtracted from the sample signal. Carbon-13 isotopes were removed and MS peaks were grouped in homologues series using a suite of Microsoft Excel macros.[62] Formula assignments were performed using the MIDAS formula calculator (http://magnet.fsu.edu/~midas/) with the following constraints applicable for deprotonated ions: C≤50, H≤100, O≤50, N≤3, and S≤1. Formulas containing both nitrogen and sulfur were not considered. Since the mobile phase contained formic acid, additional assignments allowed 1≤Na≤3 to account for sodium formate clustering. Na-containing formulas were not considered if there were too few carbon, hydrogen, or oxygen atoms to account for sodium formate. All ESI-HRMS data shown in this work correspond to neutral analyte species inferred from these assignments. The neutral formulas were characterized by the double-bond equivalent (DBE) calculated as $DBE = c - h/2 + n/2 + 1$ and aromaticity index (AI) calculated as $AI = (1 + c - o - 0.5h)/(c - o - n)$, where *c, h, o,* and *n* are the numbers of C, H, O and N atoms in the neutral formula.

3. Results and Discussion

3.1. Photosensitized Oxidation of Guaiacyl Acetone and aqSOA Formation

Fig. 1 provides an overview of the loss of GA, formation of aqSOA, and evolution of aqSOA chemical properties over the course of photoreaction. GA decays quickly upon irradiation

following pseudo-first-order kinetics with a fitted rate constant (k) of 1.28 h^{-1} and a half-life of 32.5 min (Fig. 1a). The aqSOA mass concentration increases in sync with the decrease of GA, and plateaus after ~ 3 hours of irradiation after all GA has reacted (Fig. 1b). The aqSOA mass yield is in the range of 76 ~ 91%, which is slightly lower than those reported for the photoreactions of phenol, guaiacol (2-methoxyphenol), and syringol (2, 6-dimethoxyphenol) with $^3C^*$.[42] The comparatively lower SOA yield of GA is likely due to the presence of the acetone group on its *para* position. Compared to the *meta* and *ortho* positions on phenols, the *para* position is usually more reactive for electrophilic substitution due to relatively higher electron density and less steric hindrance. Thus, the occupancy of the *para* position on GA may lower the rates of substitution reactions and reduce the production of low volatility compounds.

Previous studies reported that conjugated phenolic carbonyls (e.g., vanillin, acetovanillone, acetosyringone and syringaldehyde) undergo direct photodegradation to produce aqSOA with aqueous phase mass yields around 80%.[35,36] However, because GA absorbs weakly at wavelengths above 300 nm (Fig. S5), direct photodegradation of GA is expected to be negligible[35] compared to oxidation by $^3C^*$. Additionally, here we observed that 3,4-DMB decreases nearly linearly during illumination and 80% of the initial 3,4-DMB is lost after 5.5 hrs of irradiation (Fig. S6). No detectable loss of GA or 3,4-DMB is observed in the dark (Fig. 1a). On the other hand, consistent with previous reported aqueous photo-oxidation of guaiacol and syringol using 3,4-DMB as the source of $^3C^*$,[47] these results indicate that 3,4-DMB transforms during the oxidation of GA, and the range of products formed may potentially contain low volatility compounds. However, since the initial concentration of 3,4-DMB is 20 times lower than that of GA, the contribution of 3,4-DMB oxidation products to aqSOA is expected to be minimal. In addition, while Anastasio et al. (1997) showed that HOOH, a precursor for •OH, is produced from reactions of phenols with $^3C^*$, the amount of HOOH produced is small and •OH oxidation in the triplet experiments similar to ours appears to be negligible.[41,42] Overall, in this study GA is the dominant precursor for the observed aqSOA and the oxidation of GA is mainly driven by the triplet excited state of 3,4-DMB.

The bulk chemical composition of the aqSOA evolves continuously during illumination and becomes increasingly more oxidized (Fig. 1c). The O/C ratio of the aqSOA increases from 0.43 to 0.67 while the H/C ratio decreases from 1.60 to 1.41, leading to a rise of OS_C from –0.75 to –0.074 over ~ 6 hours of photoreaction. Note that H/C, O/C and OS_C are not reported for the first 24 min

of the reactions because of insufficient aqSOA mass. Both the O/C and H/C ratios of the aqSOA are higher than those of the precursor (O/C = 0.3 and H/C = 1.2 for GA), suggesting the occurrence of hydrogen incorporation and oxygenation pathways such as electrophilic addition of the OH radical to the aromatic ring and carboxylic acid formation. Previous studies have shown that the reactions of $^3C^*$ with phenols form H_2O_2 [41] which can be a source of OH radical. In this work, AMS tracer ions for hydroxylated GA compounds, such as $C_{10}H_{12}O_4^+$ and $C_{10}H_{12}O_5^+$, are observed in the mass spectra of the aqSOA. In addition, LC-MS analysis detects the presence of hydroxylated products of GA in the aqSOA, such as $C_{10}H_{12}O_6$, which is identified as a product of GA resulting from the addition of three OH groups to the aromatic ring (Table 1). This is consistent with previous findings that OH radical addition is an important pathway in aqueous-phase oxidation of phenols.[36,45–47,63,64]

Significant formation of carboxylic acids during the photoreaction of GA is suggested by the Van Krevelen diagram of H/C vs. O/C,[65] where the aqSOA evolves along a slope of around −1 over the course of the photooxidation (Fig. S7). The CHO_2^+ ion in the aqSOA AMS spectra, which is an indicator for the carboxyl functional group, also rises constantly over the course of the photoreaction (Fig. 1d). Furthermore, IC analysis of offline samples indicates continuous formation of five small organic acids (formic acid, acetic acid, malic acid, malonic acid, and oxalic acid) in the aqSOA (Fig. 1d), with acetic acid, formic acid, and oxalic acid being the major small acid products. In the later periods of the photoreaction (~ 5.5 hrs), the measured total small acids account for 10.9% of the original organic carbon mass. In addition, there is a tight correlation between the total concentration of organic acids measured by IC and the organic-equivalent concentration of CHO_2^+ measured by AMS. Together, these results indicate that carboxylic acids are important reaction products from the photooxidation of GA.

3.2. Photochemical Evolution of GA aqSOA Composition and Light Absorption

3.2.1. Formation and Evolution of Three Generations of aqSOA

To investigate the chemical evolution of aqSOA, we performed PMF analysis of the AMS spectra and resolved three distinct factors that are referred to as different generations of the aqSOA products. Fig. 2 shows the mass spectra of the aqSOA factors and their evolution as a function of irradiation time. The least oxidized factor (O/C = 0.42 and H/C = 1.68; Fig. 2c1) appears to

represent the first generation aqSOA products. It rises rapidly at the beginning of the illumination with an initial formation rate of 3.5 mg L^{-1} h^{-1} and gradually declines after peaking at 42 min (Fig. 2a). The 1st generation products dominate aqSOA composition within the first hour of the photoreaction but their contribution then decreases and disappears once the precursor is completely depleted (Fig. 2b). Oligomerization appears to be a prominent process in the formation of the 1st generation aqSOA materials from GA as this factor correlates tightly with $C_{20}H_{22}O_6^+$ (m/z 358) and $C_{18}H_{19}O_5^+$ (m/z 315), which are AMS tracer ions for GA dimers (Fig. 2a). Specifically, $C_{20}H_{22}O_6^+$ is the molecular ion of the GA dimer and $C_{18}H_{19}O_5^+$ is a major fragment ion of the dimer (after losing -C_2H_3O from the molecular ion). In addition, the LC-PDA-ESI/HRMS analysis of the samples collected at 15 – 33 min and 65-82 min of irradiation, confirms the presence of molecules representative of GA dimer and trimer products (e.g. $C_{20}H_{22}O_6$, $C_{20}H_{22}O_7$, $C_{20}H_{22}O_8$, $C_{20}H_{22}O_9$, $C_{30}H_{32}O_9$, and $C_{30}H_{32}O_{10}$ - see Fig. 3 panel a1 and a2).

The 2nd generation aqSOA is more oxidized (O/C = 0.56, H/C = 1.46) and presents a time trend which starts to rise after 23 min of illumination and increases at a slower rate and peaks at a later time than the 1st generation aqSOA (Fig. 2a). In the mass spectrum of this factor, the dimer molecular ion ($C_{20}H_{22}O_6^+$) disappears and the relative intensity of $C_{18}H_{19}O_5^+$ is substantially reduced (Fig. 2c2). However, smaller fragment ions from dimer derivatives, such as $C_{18}H_{17}O_5^+$ (m/z 313), $C_{15}H_{11}O_4^+$ (m/z 255) and $C_{14}H_{11}O_3^+$ (m/z 227), become more prominent (Fig. 2c). $C_{18}H_{17}O_5^+$ is likely produced from the demethylation and demethoxylation products of the GA dimer, whereas $C_{15}H_{11}O_4^+$ and $C_{14}H_{11}O_3^+$ are probably produced from the functionalized products of GA monomer or ring opening products of GA dimers. These results, as well as the similarities in the time trends of 2nd generation aqSOA and $C_{18}H_{17}O_5^+$ (Fig. 2a), suggest that the 1st generation products are transformed via hydroxylation, demethylation, demethoxylation, and partial ring-opening to form functionalized monomers and dimers (Scheme S1). Indeed, the molecules identified in the sample collected between 68 – 82 min of irradiation, which is composed of ~ 40% 1st generation and 60% 2nd generation aqSOA, show a wider range of MW and OS_C values than those in the 15 – 33 min sample, which is composed completely of 1st generation aqSOA (Fig. 3). These results suggest that oligomerization and functionalization may occur in parallel and compete in the early stages of the photoreaction, although oligomerization is more predominant at the very beginning of the photoreaction, likely because such reactions are more favored under higher precursor concentrations.

The 3rd generation aqSOA starts to rise after ~ 1 hour of irradiation and continues to increase over the entire period of irradiation (Fig. 2a). It is the most oxidized of the three identified aqSOA factors (O/C of 0.68 and H/C of 1.46) and contains the lowest fraction of ions with m/z > 100. The mass spectrum of this factor is overall similar to the semivolatile oxygenated organic aerosols (SV-OOA) commonly observed in the atmosphere.[60] Furthermore, the concentration of this factor correlates very well with the mass spectral signals of highly oxygenated smaller ions such as $C_4H_5O_3^+$ (m/z = 101; r^2 = 0.96), $CH_3O_2^+$ (m/z = 47; r^2 = 0.94) and CHO_2^+ (m/z = 45; r^2 = 0.98) (Fig. S8), suggesting that fragmentation is a major pathway in the later periods of the photochemical reactions. Also, the good correlation (r^2 = 0.88; Fig. S8) between the time trends of the 3rd generation aqSOA and the IC-measured total acid concentration suggests that carboxylic acid formation plays an important role in the later periods of the reactions. This is consistent with the HPLC-PDA-HRMS results for the final time point (313-345 min), which is almost completely 3rd generation aqSOA (Fig. 2b), and shows increased abundance of small molecules (e.g. $C_4H_4O_4$, $C_5H_6O_4$, $C_6H_6O_2$, $C_6H_8O_3$, and $C_6H_{10}O_3$). These results are also consistent with previous finds that, in phenolic aqSOA production, fragmentation can occur through demethoxylation and the cleavage of aromatic rings,[36,45,46,66] and lead to the formation of ketones, carboxylic acids, and other highly oxygenated aliphatic products. Fragmentation may convert aqSOA species into semi-volatile and volatile molecules. However, in this study, we did not observe a decrease of aqSOA mass yield in the 6 hrs of irradiation. It suggests that even in the late period of the photoreaction, the production of low-volatility compounds in the aqSOA outweights the loss of semi-volatile and volatile species. Also, it may suggest that some of the low-volatility products in the aqSOA are quite recalcitrant to fragmentation.

3.2.2. Photochemical Evolution of the Molecular Composition of aqSOA

The molecular compositions of aqSOA sampled during three time periods of irradiation, i.e., 15-33 min, 65-82 min, and 313-345 min, were analyzed using LC-PDA-ESI/HRMS.[55,67,68] Fig. 3, panels a1-a3 show all the assigned features in the aqSOA mass spectra. The identified compounds include the hydroxylation products of GA (e.g., $C_{10}H_{12}O_4$, $C_{10}H_{12}O_5$, and $C_{10}H_{12}O_6$), GA dimers (e.g., $C_{20}H_{22}O_6$, $C_{20}H_{22}O_7$, $C_{20}H_{22}O_8$, and $C_{20}H_{22}O_9$), and GA trimers (e.g., $C_{30}H_{32}O_9$, $C_{30}H_{32}O_{10}$).

Fig. 4 shows the distributions of OS_C and carbon number (n_C) of all the CHO compounds identified by the LC-PDA-ESI/HRMS in the aqSOA samples. The aqSOA formed during the initial stages of photoreaction (i.e., in 15-33 min and 65-82 min samples) contains a significant number of large molecules with n_C >20 and OS_C > -1, while the aqSOA composition towards the end of the reaction (i.e., in the 313-345 min sample) contains more smaller molecules with n_C < 10. The abundance of large molecules (n_C > 20) significantly decreases at the end of the photoreaction. The van Krevelen diagrams of the aqSOA samples (Fig. 3b1-b3) illustrate the molecular transformation of the aqSOA components. For all three samples a majority of the detected species are located in the region of O/C ≤ 1.0 and H/C ≤ 2.0. Molecules with H/C ≤ 1.0 and O/C ≤ 0.5 are typical for aromatic species, while molecules with H/C ≥ 1.5 and O/C ≤ 0.5 correspond to more aliphatic compounds.[69,70] DBE values of the aqSOA products cover a wide range, from 1 to 17. Fig. 3 panels b1-b3 indicate that products with high AI dominate at the initial stages of the photoreaction, but decrease in later periods. In particular, compounds with extremely high unsaturation degrees, such as $C_{30}H_{30}O_{10}$ (AI = 0.30), $C_{30}H_{32}O_9$ (AI = 0.29), $C_{30}H_{32}O_{10}$ (AI = 0.25) and $C_{28}H_{28}O_9$ (AI = 0.32), are only observed in the aqSOA sample irradiated for 65-82 min, and disappeared at the end of the photoreaction.

The signal-weighted average molecular formulas of the molecules detected by LC-PDA-ESI/HRMS are calculated to be $C_{15.8}H_{17.5}O_{5.5}$ in the 15-33 min sample, $C_{18.8}H_{20.7}O_{5.9}$ in the 65-82 min sample, and $C_{12.8}H_{14.9}O_{5.1}$ in the 313-345 min sample. The changes of n_C in these three samples are consistent with the AMS findings that oligomers are formed at initial stages of the reaction and small fragmentation products are more predominant in late periods. Also, consistent with the AMS findings of a continuous increase of aqSOA oxidation over the course of photoreaction, the signal-weighted average O/C ratio of the aqSOA molecules are found to increase from 0.35 to 0.40. Note that the signal-weighted average O/C ratios of aqSOA determined by the LC-PDA-ESI/HRMS are systematically lower than the average O/C ratio measured by the AMS, probably due to the difference between the ESI/HRMS and AMS methodology in terms of sample analysis, data processing, and O/C calculations.[46] Overall, these results indicate that oligomerization and functionalization dominate in early stages of the photoreaction, contributing significantly to the composition of aqSOA, while fragmentation becomes more important after prolonged photochemical aging, leading to the formation of highly oxidized smaller species. Nevertheless,

some high MW oligomeric compounds appear to be recalcitrant to photoreaction and can survive after 5 hours of irradiation (Fig. 3a3).

3.2.3. Light Absorbance by aqSOA

During illumination, the aqueous solution changed from colorless to yellow, indicating the formation of light-absorbing compounds (i.e., BrC). Fig. 5 shows the absorption coefficient (cm^{-1}) and the mass absorption coefficient (MAC, $cm^2\ g^{-1}$) of the aqSOA in the wavelength range of 300-550 nm (the absorbance due to GA and 3,4-DMB has been removed). The aqSOA UV-vis absorption spectra exhibit general exponential shapes in the range of 300-550 nm. The calculated MAC values at 350 nm are in the range of 4300 and 8800 cm^2g^{-1}, similar to the MAC values previously reported for phenolic aqSOA.[35] Absorption Angstrom Exponents (AAE) for the illuminated reaction solution increases from 5.1 (± 0.48) to 9.4 ((± 0.15) (Fig. 5 and Fig. S9). The AAE values measured in this study are similar to the previous values observed for BrC from biomass burning.[71,72] Also, the increasing trend of the AAE value during the photoreaction indicates that the wavelength-dependence of the absorption of the aqSOA becomes more pronounced as reactions progress.

Both the absorption coefficient and the MAC of the aqSOA increase with time at the beginning of the photoreactions but decrease slightly in later periods (Fig. 5). This trend is more clearly shown in the plot of the sunlight absorption rate (R_{abs}) of aqSOA as a function of irradiation time (Fig. 6). In the first 3 hours of irradiation, the R_{abs} increases 4.6 folds from 7.1×10^{-7} ($\pm\ 1.1\times10^{-8}$) to 3.3×10^{-6} ($\pm\ 1.1\times10^{-8}$) mol-photons $L^{-1}s^{-1}$, and the aqSOA-mass-normalized R_{abs} increases 1.7 folds from 1.2×10^{-7} ($\pm\ 1.9\times10^{-9}$) to 2.1×10^{-7} ($\pm\ 7.1\times10^{-10}$) mol-photons $mg^{-1}s^{-1}$. During the same period, the total concentration of the 1st and 2nd generation aqSOA products rises and reaches a maximum, indicating that the formation of GA oligomers and functionalized products contributes to the formation of chromophores. From 3 to 6 hours of irradiation, the R_{abs} of the aqSOA decreases by 20% while the total aqSOA mass remains constant (Fig. 6), resulting in a 20% decrease of the mass normalized R_{abs} (from 2.1×10^{-7} to 1.7×10^{-7} mol-photons $mg^{-1}s^{-1}$). This decrease of the aqSOA light absorption correlates with a continuous increase of the 3rd generation aqSOA products, which are composed of a higher mass fraction of smaller fragmentation products compared to the 1st and

the 2nd generation aqSOA. This is an indication that the transformation of the early generation products may cause the degradation of chromophores and an overall photobleaching of the aqSOA.

3.3. Molecular Characterization of BrC in GA aqSOA

Table 1 summarizes the UV-vis spectra, chemical structures, and proposed formation mechanisms of the major BrC chromophores identified using HPLC-PDA-HRMS. Hydroxylation and dimerization of GA appear to be important pathways in the formation of chromophores. GA (#5 in Table 1) shows significant absorption around 280 nm but nearly no absorption in the solar range (i.e., above 290 nm). However, hydroxylated GA ($C_{10}H_{12}O_6$, #3 in Table 1) show strong light absorbance at wavelengths above 290 nm and exhibit a significant absorption band around 310 nm. Three dimerization products of GA (#9, 10 and 11 in Table 1) formed through C-C linkage were identified, which exhibit significant absorption bands at wavelengths around 320, 330, and 390 nm. Here, since C-O dimerization can break the conjugation system and would produce less absorbing products, thus the detected BrC chromophores are more likely to be C-C dimers rather than C-O dimers. $C_{19}H_{22}O_6$ (#11 in Table 1) could be a derivative of $C_{20}H_{22}O_7$ (#9 in Table 1) produced from Norrish photochemical reaction with a loss of CO.[73] Hydroxylation and dimerization of GA can extend the conjugation of the π-bonds in the aromatic ring, causing red shifts of the absorption bands. In addition, hydroxylation and dimerization of DMB also contribute to the chromophore formation in this study (#1, 4, and 8 in Table 1). Although the products from DMB-participated reactions are only a minor contributor to the aqSOA mass due to the low initial DMB concentration, the contribution of DMB products to the absorption of aqSOA may still be important.

Using LC-PDA-ESI/HRMS, some of the structural isomers with the same formula can be separated on the LC column. For a significant number of the assigned formulas, structural isomers were observed and some of them undergo different transformations during the photoreaction. For example, $C_{20}H_{22}O_6$ shows three isomers eluted at retention time (RT) values of 20.3 min, 20.9 min, and 24.5 min, respectively. Possible structures for $C_{20}H_{22}O_6$ may include GA dimers and other species such as derivatives of GA functionalized products and oligomers. $C_{20}H_{22}O_6$ (RT = 20.3 min) and $C_{20}H_{22}O_6$ (RT 20.9 = min) were observed at the very beginning of the reaction, but quickly disappeared. $C_{20}H_{22}O_6$ (RT = 24.5 min, #11 in Table 1) was not present at the very

beginning of the reaction, but was observed in later samples and decreased with prolonged reactions time. Previous studies on phenolic aqSOA formation have suggested that phenolic dimers can be formed through C-C or C-O coupling of phenoxy radicals produced via H-abstraction of the phenol or via OH-addition to the aromatic ring.[36,45,46,74] Further, for GA, the reaction could occur at the *meta* or *ortho* positions to the hydroxyl group. The observed structural isomers of $C_{20}H_{22}O_6$ could therefore be guaiacyl acetone dimers formed through different mechanisms, and may also be other structural isomers.

4. Atmospheric Implication

This study reveals that the aqueous-phase photosensitized reaction of GA, a phenolic carbonyl emitted from wood burning, can be an effective source of aqSOA and BrC. The fast reaction rate and high aqSOA yield of GA suggest that aqueous-phase photosensitized reactions of phenolic carbonyls in biomass burning emissions may play an important role in atmospheric SOA production. Our results show that oligomerization and functionalization dominate in the early stages of the reaction, while fragmentation becomes increasingly more important with prolonged aging. This finding is consistent with prior studies, which have also observed oligomerization, functionalization and fragmentation competing in aqSOA formation during photodegradation of phenols.[45–47] The O/C ratio of the GA-derived aqSOA increases from 0.42 to 0.67, and the OS_C increases from − 0.75 to − 0.073 over the 5.6 hrs of photoreaction. The significant increases in the O/C ratio and OS_C of aqSOA compared to the precursor indicate that aqueous processing of GA and similar phenols could be an effective source of oxygenated organic aerosols (OOA) in areas impacted by biomass burning emissions. In addition, BrC compounds, which mainly include GA oligomers and functionalized products, are formed at the initial stages of the photosensitized reaction of GA. The light absorption of the aqSOA in the range of 300 – 550 nm increases initially, when the 1st generation aqSOA dominates the composition, reaches a plateau as the aqSOA composition is primarily composed of 2nd and 3rd generation products, and decreases slightly by the end of the reaction when the aqSOA is composed completely of the 3rd generation products. This finding may help elucidating how phenolic aqSOA influences the radiative balance of the atmosphere, and may have important implications for understanding the climate impacts of phenolic aqSOA during atmospheric aging.

Supporting Information

Schematic of the RPR-200 photoreactor and the distribution of the photon flux inside the photoreactor (Figure S1); correlation between the organic H_2O^+ signal and the CO_2^+ signal measured by AMS (Figure S2); diagnostic plots for the four-factor solution for the PMF analysis (Figure S3); mass concentration and fraction time series and MS profile of the background factor obtained from the PMF analysis (Figure S4); UV-vis absorption spectrum of GA standard (Figure S5); loss of 3,4-DMB in the reaction solution (Figure S6); Van Krevelen diagram and triangle plot of the aqSOA obtained from AMS measurements (Figure S7); correlations between selected ions and the 3rd generation products factor obtained from the PMF analysis (Figure S8); time series of the AAE of the illuminated reaction solution (Figure S9); possible products produced during the aqueous-phase photooxidation of GA (Scheme S1)

Acknowledgements

This work was supported by the U.S. National Science Foundation, Grant No. AGS-1649212 and the California Agricultural Experiment Station (Projects CA-D-ETX-2102-H and CA-D-LAW-6403-RR). PU group acknowledges additional support from discretional startup funds allocated to A.L. WJ and AM acknowledge additional funding from the Jastro-Shields Graduate Research Award and the Donald G. Crosby Fellowship at UC Davis.

Figures

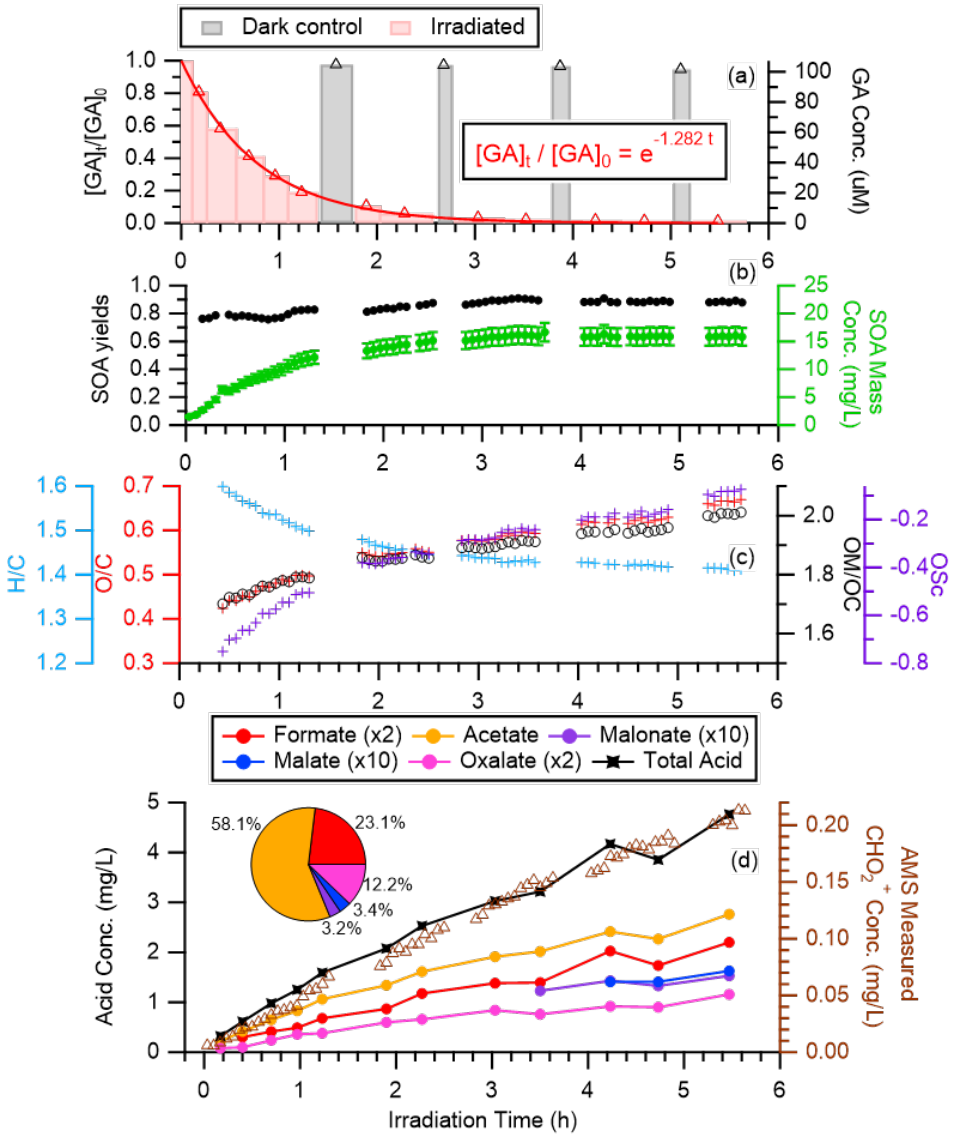

Figure 1. Overview of the aqueous photoreaction of guaiacyl acetone (GA) with the triplet excited state of 3,4-DMB and aqSOA formation over the course of simulated sunlight illumination. (a) Apparent first-order decay of GA measured by HPLC in offline samples. $[GA]_0$ and $[GA]_t$ are the concentrations of GA measured initially and at time *t* of illumination. Evolution trends of (b) aqSOA concentration and mass yield (error bars represent 1σ (10%) of uncertainty in AMS quantification of aqSOA mass) and (c) H/C, O/C, OM/OC and OS_C determined by HR-ToF-AMS. Evolution trends of (d) organic-equivalent concentrations of CHO_2^+ (HR-ToF-AMS tracer ion for carboxylic acids) and concentrations of organic acids measured by IC. The total acid concentration in (d) represents the sum of the five acids and the pie chart shows the mass contributions of individual acids measured in the last offline sample. The sampling duration for each offline sample is marked on (a) and the irradiation time for each offline sample symbol is displayed as the mean of the sampling start time and end time.

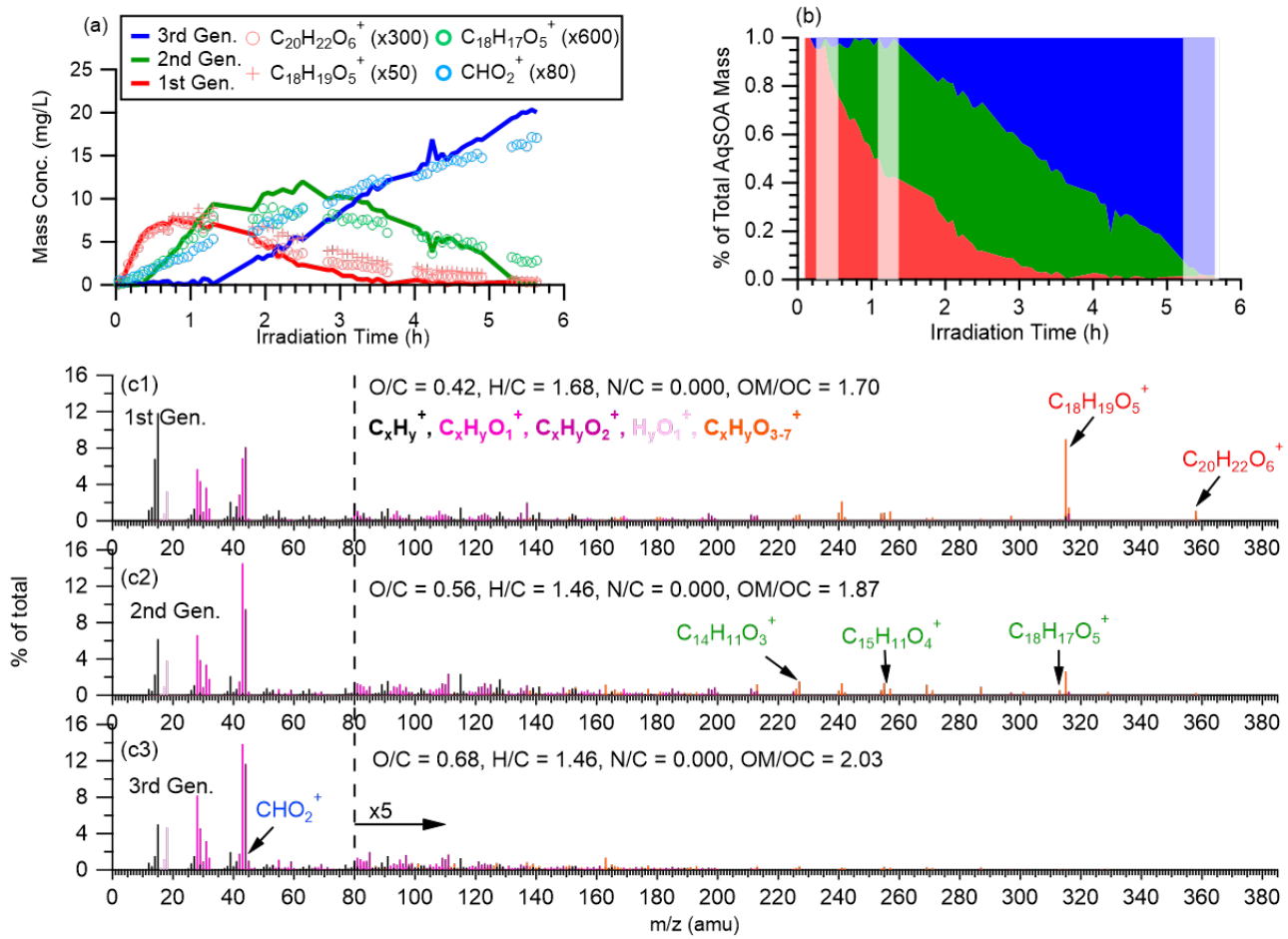

522

523 Figure 2. (a) Time series (b) fraction time series and (c) MS profiles for the three generations of
524 aqSOA products obtained from PMF analysis. The shaded areas in (b) show the offline samples
525 for LC-MS analysis. The peaks in the mass spectra are color-coded according to five ion categories:
526 $C_xH_y^+$, $C_xH_yO^+$, $C_xH_yO_2^+$, $H_yO_1^+$, $C_xH_yO_{3\text{-}7}^+$ (x>1, y$\geqslant$0). The tracer ions representative of the 1st
527 generation (red), 2nd generation (green), and 3rd generation (blue) products are marked on the mass
528 spectra in c1-c3.

529

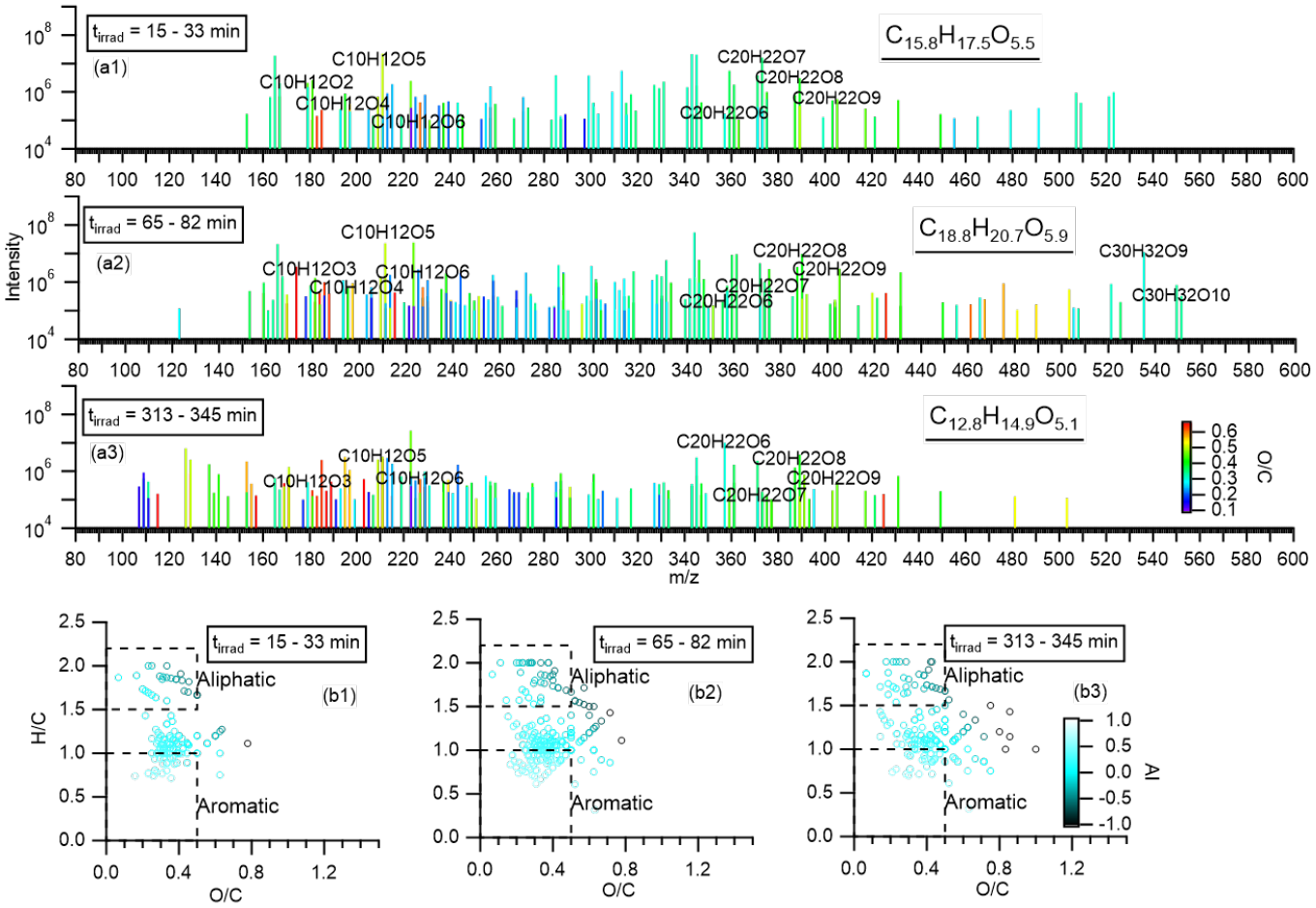

530

531 Figure 3. (a1-a3) Molecules detected by negative ion mode LC-ESI-HRMS in aqSOA samples at
532 different stages of the photoreaction. Signals are colored by the O/C ratios of the formulas. The
533 underlined molecular formular is the intensity-weighted average formular for the sample; and (b1-
534 b3) Van Krevelen diagrams of the aqSOA components formed at different stages of photoreaction.
535 Each data point is colored by the aromaticity index (AI) value of the formula.

536

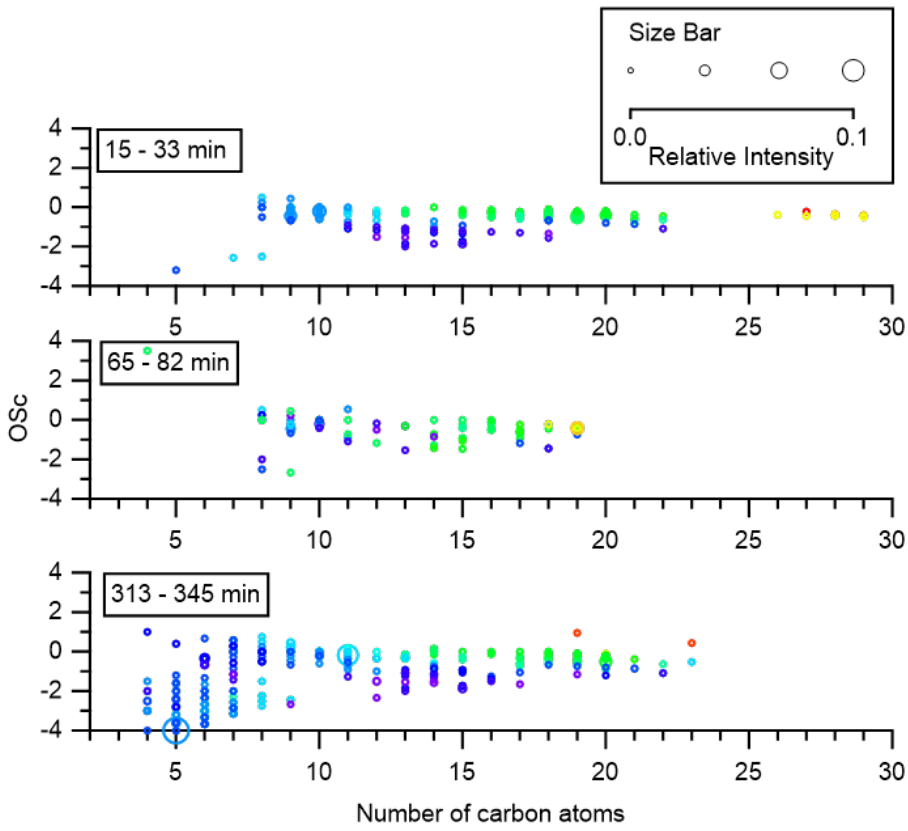

537

538 Figure 4. OSC and carbon number of chromophores detected in the irradiated samples determined
539 by LC-PDA-ESI/HRMS, colored by DBE and size by the peak relative intensity in the mass
540 spectrum (size 1-4 represents 0.0001-0.1).

541

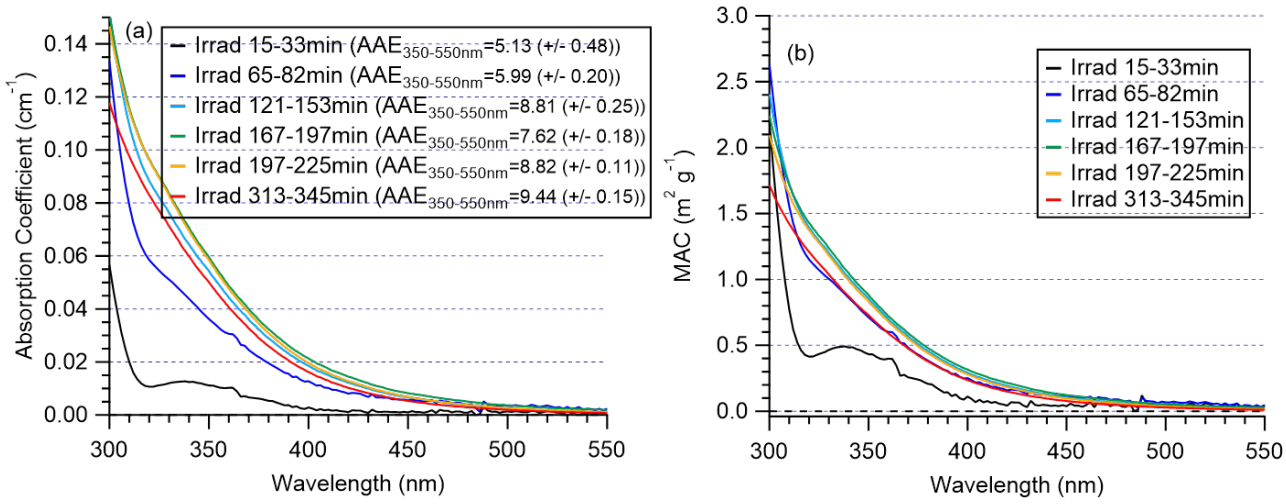

542

543 Figure 5. (a) Absorption coefficient and (b) mass absorption coefficients (MAC) of 6 offline
544 samples collected throughout the course of the photoreaction of GA with $^3C^*$ (t_0 data subtracted).
545 The AAE value for each sample is reported in the legend of (a).

546

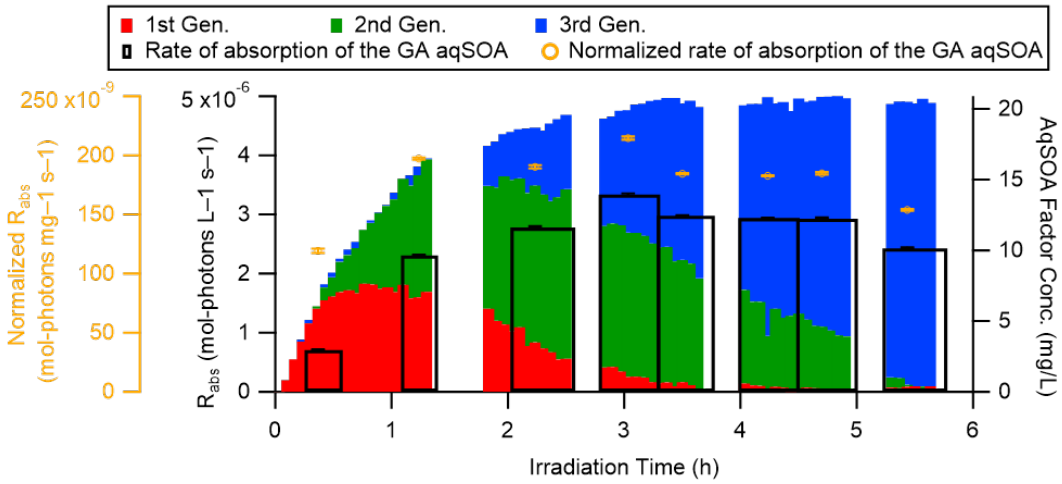

547

548 Figure 6. Change in the rate of sunlight absorption (black bars) and the organic mass normalized
549 rate of sunlight absorption (black triangles) (λ= 300-550 nm) of the aqSOA of GA as a function
550 of irradiation time, together with the time series of the three generations of aqSOA. Error bars
551 represent ±1 standard error (SE) calculated by propagating the uncertainties.

552

553 Table 1. Information for the identified aqSOA chromophores, GA, and DMB detected by LC-
554 PDA-(-)ESI-HRMS in four offline samples collected during the photoreaction. The compounds
555 are numbered in the order of their retention times. The y-axis of the UV-Vis spectrum is the
556 absorbance detected by PDA (AU).

#	UV-Vis spectrum and RT	Neutral Formula and Nominal Mass	Possible structures	Proposed Formation Mechanisms
1	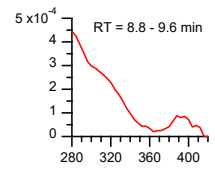	$C_7H_6O_3$, 138.0317 amu	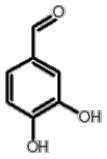	Formed by methoxy displacement of DMB. Both methoxy groups are replaced by hydroxyl groups
2	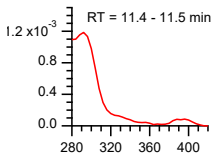	$C_8H_8O_4$, 168.0423 amu	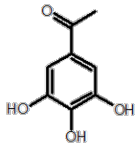	Mechanism is not apparent. Proposed structure is chosen for its stability.
3	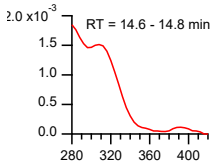	$C_{10}H_{12}O_6$, 228.0634 amu	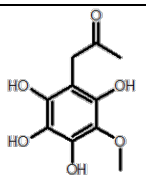	Monomeric product of GA resulting from addition of three OH radicals to the aromatic ring.
4	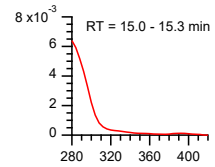	$C_9H_{10}O_3$, 166.0630 amu	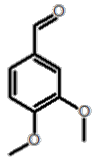	**DMB – the photosensitizer.** Source of triplet carbon used to oxidize GA.
5	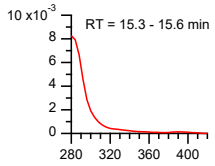	$C_{10}H_{12}O_3$, 180.0786 amu	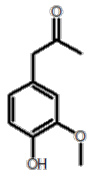	**GA – the phenol precursor.**
6	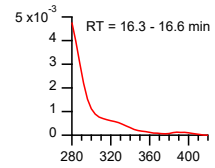	$C_{11}H_{12}O_5$, 224.0685 amu	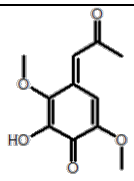	Monomeric product of GA resulting from addition of an OH radical and a methoxy radical and to the aromatic ring. Another OH radical abstracts a proton, resulting in a water byproduct. Rearrangement of double bonds to form a quinoidal system in conjugation with the ketone group.
7	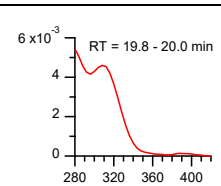	$C_{17}H_{18}O_5$, 302.1154 amu	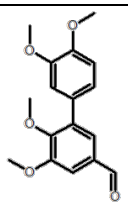	DMB+DMB dimeric product resulting from photolysis leading to the formation of CHO and dimethoxybenzyl radicals and addition to an DMB unit. Hydrogen abstraction is then achieved by OH.

8	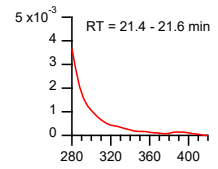	$C_{19}H_{20}O_6$, 344.1260 amu	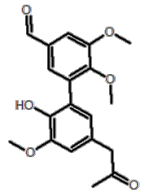	GA+DMB dimeric product formed by C-C linkage of a GA radical to a DMB unit. Hydrogen abstraction is achieved by OH.
9	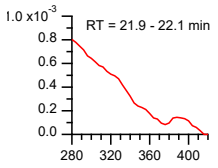	$C_{20}H_{22}O_7$, 374.1365 amu	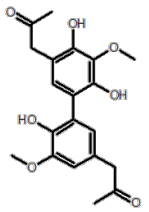	GA+GA dimeric product, formed by linking two C radicals; formed either before or after OH radical addition to one aromatic ring.
10	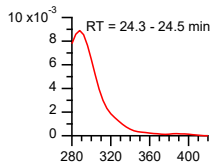	$C_{20}H_{22}O_6$, 358.1416 amu	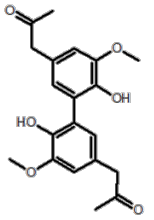	GA+GA dimeric product, formed by linking two C radicals.
11	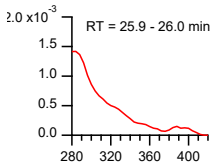	$C_{19}H_{22}O_6$, 346.1416 amu	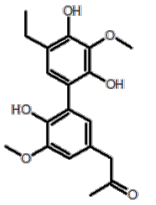	GA+GA dimeric product resulting from Norrish photochemistry with product 9. A CO unit is removed from the molecule.

557

558

Reference

(1) Schauer, J. J.; Cass, G. R. Source Apportionment of Wintertime Gas-Phase and Particle-Phase Air Pollutants Using Organic Compounds as Tracers. *Environ. Sci. Technol.* **2000**, *34* (9), 1821–1832. https://doi.org/10.1021/es981312t.

(2) De Gouw, J.; Jimenez, J. L. Organic Aerosols in the Earth's Atmosphere. *Environ. Sci. Technol.* **2009**, *43* (20), 7614–7618. https://doi.org/10.1021/es9006004.

(3) Cordell, R. L.; Mazet, M.; Dechoux, C.; Hama, S. M. L.; Staelens, J.; Hofman, J.; Stroobants, C.; Roekens, E.; Kos, G. P. A.; Weijers, E. P.; Frumau, K.F.A.; Panteliadis, P.; Delaunay, T.; Wyche, K.P.; Monks, P.S. Evaluation of Biomass Burning across North West Europe and Its Impact on Air Quality. *Atmos. Environ.* **2016**, *141*, 276–286. https://doi.org/10.1016/J.ATMOSENV.2016.06.065.

(4) Yadav, I. C.; Linthoingambi Devi, N.; Li, J.; Syed, J. H.; Zhang, G.; Watanabe, H. Biomass Burning in Indo-China Peninsula and Its Impacts on Regional Air Quality and Global Climate Change-a Review. *Environ. Pollut.* **2017**, *227*, 414–427. https://doi.org/10.1016/J.ENVPOL.2017.04.085.

(5) Sommers, W. T.; Loehman, R. A.; Hardy, C. C. Wildland Fire Emissions, Carbon, and Climate: Science Overview and Knowledge Needs. *For. Ecol. Manage.* **2014**, *317*, 1–8. https://doi.org/10.1016/j.foreco.2013.12.014.

(6) Jaffe, D. A.; O'Neill, S. M.; Larkin, N. K.; Holder, A. L.; Peterson, D. L.; Halofsky, J. E.; Rappold, A. G. Wildfire and Prescribed Burning Impacts on Air Quality in the United States. *J. Air Waste Manage. Assoc.* **2020**, *70* (6), 583–615. https://doi.org/10.1080/10962247.2020.1749731.

(7) O'Dell, K.; Ford, B.; Fischer, E. V; Pierce, J. R. Contribution of Wildland-Fire Smoke to US PM2.5 and Its Influence on Recent Trends. *Environ. Sci. Technol.* **2019**, *53* (4), 1797–1804. https://doi.org/10.1021/acs.est.8b05430.

(8) E., R. C.; Michael, B.; H., J. F.; Michael, J.; R., B. J.; T., E. C. Critical Review of Health Impacts of Wildfire Smoke Exposure. *Environ. Health Perspect.* **2016**, *124* (9), 1334–1343. https://doi.org/10.1289/ehp.1409277.

(9) Jeong, C.-H.; Evans, G. J.; Dann, T.; Graham, M.; Herod, D.; Dabek-Zlotorzynska, E.; Mathieu, D.; Ding, L.; Wang, D. Influence of Biomass Burning on Wintertime Fine Particulate Matter: Source Contribution at a Valley Site in Rural British Columbia. *Atmos. Environ.* **2008**, *42* (16), 3684–3699. https://doi.org/10.1016/J.ATMOSENV.2008.01.006.

(10) Ward, T. J.; Rinehart, L. R.; Lange, T. The 2003/2004 Libby, Montana PM2.5 Source Apportionment Research Study. *Aerosol Sci. Technol.* **2006**, *40* (3), 166–177. https://doi.org/10.1080/02786820500494536.

(11) Young, D. E.; Kim, H.; Parworth, C.; Zhou, S.; Zhang, X.; Cappa, C. D.; Seco, R.; Kim, S.; Zhang, Q. Influences of Emission Sources and Meteorology on Aerosol Chemistry in a Polluted Urban Environment: Results from DISCOVER-AQ California. *Atmos. Chem. Phys.* **2016**, *16* (8), 5427–5451. https://doi.org/10.5194/acp-16-5427-2016.

(12) Gaston, C. J.; Lopez-Hilfiker, F. D.; Whybrew, L. E.; Hadley, O.; McNair, F.; Gao, H.; Jaffe, D. A.; Thornton, J. A. Online Molecular Characterization of Fine Particulate Matter

in Port Angeles, WA: Evidence for a Major Impact from Residential Wood Smoke. *Atmos. Environ.* **2016**, *138*, 99–107. https://doi.org/https://doi.org/10.1016/j.atmosenv.2016.05.013.

(13) Sullivan, A. P.; Guo, H.; Schroder, J. C.; Campuzano-Jost, P.; Jimenez, J. L.; Campos, T.; Shah, V.; Jaeglé, L.; Lee, B. H.; Lopez-Hilfiker, F. D.; Thornton, J. A.; Brown, S. S.; Weber, R. J. Biomass Burning Markers and Residential Burning in the WINTER Aircraft Campaign. *J. Geophys. Res. Atmos.* **2019**, *124* (3), 1846–1861. https://doi.org/10.1029/2017JD028153.

(14) Ge, X.; Setyan, A.; Sun, Y.; Zhang, Q. Primary and Secondary Organic Aerosols in Fresno, California during Wintertime: Results from High Resolution Aerosol Mass Spectrometry. *J. Geophys. Res. Atmos.* **2012**, *117* (D19). https://doi.org/10.1029/2012JD018026.

(15) Chen, C.-L.; Chen, S.; Russell, L. M.; Liu, J.; Price, D. J.; Betha, R.; Sanchez, K. J.; Lee, A. K. Y.; Williams, L.; Collier, S. C.; Zhang, Q.; Kumar, A.; Kleeman, M. J.; Zhang, X.; Cappa, C. D. Organic Aerosol Particle Chemical Properties Associated With Residential Burning and Fog in Wintertime San Joaquin Valley (Fresno) and With Vehicle and Firework Emissions in Summertime South Coast Air Basin (Fontana). *J. Geophys. Res. Atmos.* **2018**, *123* (18), 10,707-710,731. https://doi.org/10.1029/2018JD028374.

(16) Knorr, W.; Dentener, F.; Lamarque, J.-F.; Jiang, L.; Arneth, A. Wildfire Air Pollution Hazard during the 21st Century. *Atmos. Chem. Phys.* **2017**, *17* (14), 9223–9236. https://doi.org/10.5194/acp-17-9223-2017.

(17) McClure, C. D.; Jaffe, D. A. US Particulate Matter Air Quality Improves except in Wildfire-Prone Areas. *Proc. Natl. Acad. Sci.* **2018**, *115* (31), 7901 LP – 7906. https://doi.org/10.1073/pnas.1804353115.

(18) Xie, M.; Chen, X.; Hays, M. D.; Holder, A. L. Composition and Light Absorption of N-Containing Aromatic Compounds in Organic Aerosols from Laboratory Biomass Burning. *Atmos. Chem. Phys.* **2019**, *19* (5), 2899–2915. https://doi.org/10.5194/acp-19-2899-2019.

(19) Adler, G.; Wagner, N. L.; Lamb, K. D.; Manfred, K. M.; Schwarz, J. P.; Franchin, A.; Middlebrook, A. M.; Washenfelder, R. A.; Womack, C. C.; Yokelson, R. J.; Murphy, D. M. Evidence in Biomass Burning Smoke for a Light-Absorbing Aerosol with Properties Intermediate between Brown and Black Carbon. *Aerosol Sci. Technol.* **2019**, *53* (9), 976–989. https://doi.org/10.1080/02786826.2019.1617832.

(20) Fleming, L. T.; Lin, P.; Roberts, J. M.; Selimovic, V.; Yokelson, R.; Laskin, J.; Laskin, A.; Nizkorodov, S. A. Molecular Composition and Photochemical Lifetimes of Brown Carbon Chromophores in Biomass Burning Organic Aerosol. *Atmos. Chem. Phys. Discuss.* **2019**, *2019*, 1–38. https://doi.org/10.5194/acp-2019-523.

(21) Scott, A. F.; Reilly, C. A. Wood and Biomass Smoke: Addressing Human Health Risks and Exposures. *Chem. Res. Toxicol.* **2019**, *32* (2), 219–221. https://doi.org/10.1021/acs.chemrestox.8b00318.

(22) Bruns, E. A.; El Haddad, I.; Slowik, J. G.; Kilic, D.; Klein, F.; Baltensperger, U.; Prévôt, A. S. H. Identification of Significant Precursor Gases of Secondary Organic Aerosols from Residential Wood Combustion. **2016**, *6*, 27881. https://doi.org/10.1038/srep27881.

(23) Gilardoni, S.; Massoli, P.; Paglione, M.; Giulianelli, L.; Carbone, C.; Rinaldi, M.; Decesari, S.; Sandrini, S.; Costabile, F.; Gobbi, G. P.; Pietrogrande, M. C.; Visentin, M.; Scotto, F.; Fuzzi, S.; Facchini, M. C. Direct Observation of Aqueous Secondary Organic Aerosol from Biomass-Burning Emissions. *Proc. Natl. Acad. Sci.* **2016**, *113* (36), 10013–10018. https://doi.org/10.1073/pnas.1602212113.

(24) Liu, C.; Liu, J.; Liu, Y.; Chen, T.; He, H. Secondary Organic Aerosol Formation from the OH-Initiated Oxidation of Guaiacol under Different Experimental Conditions. *Atmos. Environ.* **2019**, *207*, 30–37. https://doi.org/10.1016/j.atmosenv.2019.03.021.

(25) Hatch, L. E.; Yokelson, R. J.; Stockwell, C. E.; Veres, P. R.; Simpson, I. J.; Blake, D. R.; Orlando, J. J.; Barsanti, K. C. Multi-Instrument Comparison and Compilation of Non-Methane Organic Gas Emissions from Biomass Burning and Implications for Smoke-Derived Secondary Organic Aerosol Precursors. *Atmos. Chem. Phys.* **2017**, *17* (2), 1471–1489. https://doi.org/10.5194/acp-17-1471-2017.

(26) Gilman, J. B.; Lerner, B. M.; Kuster, W. C.; Goldan, P. D.; Warneke, C.; Veres, P. R.; Roberts, J. M.; de Gouw, J. A.; Burling, I. R.; Yokelson, R. J. Biomass Burning Emissions and Potential Air Quality Impacts of Volatile Organic Compounds and Other Trace Gases from Fuels Common in the US. *Atmos. Chem. Phys.* **2015**, *15* (24), 13915–13938. https://doi.org/10.5194/acp-15-13915-2015.

(27) Zhong, M.; Jang, M. Dynamic Light Absorption of Biomass-Burning Organic Carbon Photochemically Aged under Natural Sunlight. *Atmos. Chem. Phys.* **2014**, *14* (3), 1517–1525. https://doi.org/10.5194/acp-14-1517-2014.

(28) Cappa, C. D.; Lim, C. Y.; Hagan, D. H.; Coggon, M.; Koss, A.; Sekimoto, K.; de Gouw, J.; Onasch, T. B.; Warneke, C.; Kroll, J. H. Biomass-Burning-Derived Particles from a Wide Variety of Fuels – Part 2: Effects of Photochemical Aging on Particle Optical and Chemical Properties. *Atmos. Chem. Phys.* **2020**, *20* (14), 8511–8532. https://doi.org/10.5194/acp-20-8511-2020.

(29) Hems, R. F.; Schnitzler, E. G.; Bastawrous, M.; Soong, R.; Simpson, A. J.; Abbatt, J. P. D. Aqueous Photoreactions of Wood Smoke Brown Carbon. *ACS Earth Sp. Chem.* **2020**, *4* (7), 1149–1160. https://doi.org/10.1021/acsearthspacechem.0c00117.

(30) Pang, H.; Zhang, Q.; Lu, X.; Li, K.; Chen, H.; Chen, J.; Yang, X.; Ma, Y.; Ma, J.; Huang, C. Nitrite-Mediated Photooxidation of Vanillin in the Atmospheric Aqueous Phase. *Environ. Sci. Technol.* **2019**, *53* (24), 14253–14263. https://doi.org/10.1021/acs.est.9b03649.

(31) Li, C.; He, Q.; Schade, J.; Passig, J.; Zimmermann, R.; Meidan, D.; Laskin, A.; Rudich, Y. Dynamic Changes in Optical and Chemical Properties of Tar Ball Aerosols by Atmospheric Photochemical Aging. *Atmos. Chem. Phys.* **2019**, *19* (1), 139–163. https://doi.org/10.5194/acp-19-139-2019.

(32) Simpson, C. D.; Paulsen, M.; Dills, R. L.; Liu, L.-J. S.; Kalman, D. A. Determination of Methoxyphenols in Ambient Atmospheric Particulate Matter: Tracers for Wood Combustion. *Environ. Sci. Technol.* **2005**, *39* (2), 631–637. https://doi.org/10.1021/es0486871.

(33) Schauer, J. J.; Kleeman, M. J.; Cass, G. R.; Simoneit, B. R. T. Measurement of Emissions

from Air Pollution Sources. 3. C1−C29 Organic Compounds from Fireplace Combustion of Wood. *Environ. Sci. Technol.* **2001**, *35* (9), 1716–1728. https://doi.org/10.1021/es001331e.

(34) McFall, A. S.; Johnson, A. W.; Anastasio, C. Air–Water Partitioning of Biomass-Burning Phenols and the Effects of Temperature and Salinity. *Environ. Sci. Technol.* **2020**, *54* (7), 3823–3830. https://doi.org/10.1021/acs.est.9b06443.

(35) Smith, J. D.; Kinney, H.; Anastasio, C. Phenolic Carbonyls Undergo Rapid Aqueous Photodegradation to Form Low-Volatility, Light-Absorbing Products. *Atmos. Environ.* **2016**, *126*, 36–44. https://doi.org/http://dx.doi.org/10.1016/j.atmosenv.2015.11.035.

(36) Huang, D. D.; Zhang, Q.; Cheung, H. H. Y.; Yu, L.; Zhou, S.; Anastasio, C.; Smith, J. D.; Chan, C. K. Formation and Evolution of AqSOA from Aqueous-Phase Reactions of Phenolic Carbonyls: Comparison between Ammonium Sulfate and Ammonium Nitrate Solutions. *Environ. Sci. Technol.* **2018**. https://doi.org/10.1021/acs.est.8b03441.

(37) Chang, J. L.; Thompson, J. E. Characterization of Colored Products Formed during Irradiation of Aqueous Solutions Containing H2O2 and Phenolic Compounds. *Atmos. Environ.* **2010**, *44* (4), 541–551. https://doi.org/10.1016/J.ATMOSENV.2009.10.042.

(38) Li, Y. J.; Huang, D. D.; Cheung, H. Y.; Lee, A. K. Y.; Chan, C. K. Aqueous-Phase Photochemical Oxidation and Direct Photolysis of Vanillin – a Model Compound of Methoxy Phenols from Biomass Burning. *Atmos. Chem. Phys.* **2014**, *14* (6), 2871–2885. https://doi.org/10.5194/acp-14-2871-2014.

(39) Nolte, C. G.; Schauer, J. J.; Cass, G. R.; Simoneit, B. R. T. Highly Polar Organic Compounds Present in Wood Smoke and in the Ambient Atmosphere. *Environ. Sci. Technol.* **2001**, *35* (10), 1912–1919. https://doi.org/10.1021/es001420r.

(40) Feigenbrugel, V.; Le Calvé, S.; Mirabel, P.; Louis, F. Henry's Law Constant Measurements for Phenol, o-, m-, and p-Cresol as a Function of Temperature. *Atmos. Environ.* **2004**, *38* (33), 5577–5588. https://doi.org/10.1016/j.atmosenv.2004.06.025.

(41) Anastasio, C.; Faust, B. C.; Rao, C. J. Aromatic Carbonyl Compounds as Aqueous-Phase Photochemical Sources of Hydrogen Peroxide in Acidic Sulfate Aerosols, Fogs, and Clouds. 1. Non-Phenolic Methoxybenzaldehydes and Methoxyacetophenones with Reductants (Phenols). *Environ. Sci. Technol.* **1997**, *31* (1), 218–232. https://doi.org/10.1021/es960359g.

(42) Smith, J. D.; Sio, V.; Yu, L.; Zhang, Q.; Anastasio, C. Secondary Organic Aerosol Production from Aqueous Reactions of Atmospheric Phenols with an Organic Triplet Excited State. *Environ. Sci. Technol.* **2014**, *48* (2), 1049–1057. https://doi.org/10.1021/es4045715.

(43) Kaur, R.; Labins, J. R.; Helbock, S. S.; Jiang, W.; Bein, K.; Zhang, Q.; Anastasio, C. Photooxidants from Brown Carbon and Other Chromophores in Illuminated Particle Extracts. *Atmos. Chem. Phys. Discuss.* **2018**, *2018*, 1–34. https://doi.org/10.5194/acp-2018-1258.

(44) Smith, J. D.; Kinney, H.; Anastasio, C. Aqueous Benzene-Diols React with an Organic Triplet Excited State and Hydroxyl Radical to Form Secondary Organic Aerosol. *Phys. Chem. Chem. Phys.* **2015**, *17* (15), 10227–10237. https://doi.org/10.1039/C4CP06095D.

(45) Sun, Y. L.; Zhang, Q.; Anastasio, C.; Sun, J. Insights into Secondary Organic Aerosol Formed via Aqueous-Phase Reactions of Phenolic Compounds Based on High Resolution Mass Spectrometry. *Atmos. Chem. Phys.* **2010**, *10* (10), 4809–4822. https://doi.org/10.5194/acp-10-4809-2010.

(46) Yu, L.; Smith, J.; Laskin, A.; Anastasio, C.; Laskin, J.; Zhang, Q. Chemical Characterization of SOA Formed from Aqueous-Phase Reactions of Phenols with the Triplet Excited State of Carbonyl and Hydroxyl Radical. *Atmos. Chem. Phys.* **2014**, *14* (24), 13801–13816. https://doi.org/10.5194/acp-14-13801-2014.

(47) Yu, L.; Smith, J.; Laskin, A.; George, K. M.; Anastasio, C.; Laskin, J.; Dillner, A. M.; Zhang, Q. Molecular Transformations of Phenolic SOA during Photochemical Aging in the Aqueous Phase: Competition among Oligomerization, Functionalization, and Fragmentation. *Atmos. Chem. Phys.* **2016**, *16* (7), 4511–4527. https://doi.org/10.5194/acp-16-4511-2016.

(48) Simoneit, B. R. T. A Review of Biomarker Compounds as Source Indicators and Tracers for Air Pollution. *Environ. Sci. Pollut. Res.* **1999**, *6* (3), 159–169. https://doi.org/10.1007/bf02987621.

(49) Kaur, R.; Labins, J. R.; Helbock, S. S.; Jiang, W.; Bein, K. J.; Zhang, Q.; Anastasio, C. Photooxidants from Brown Carbon and Other Chromophores in Illuminated Particle Extracts. *Atmos. Chem. Phys.* **2019**, *19* (9), 6579–6594. https://doi.org/10.5194/acp-19-6579-2019.

(50) Kaur, R.; Anastasio, C. First Measurements of Organic Triplet Excited States in Atmospheric Waters. *Environ. Sci. Technol.* **2018**, *52* (9), 5218–5226. https://doi.org/10.1021/acs.est.7b06699.

(51) Collett, J. L.; Hoag, K. J.; Sherman, D. E.; Bator, A.; Richards, L. W. Spatial and Temporal Variations in San Joaquin Valley Fog Chemistry. *Atmos. Environ.* **1998**, *33* (1), 129–140. https://doi.org/https://doi.org/10.1016/S1352-2310(98)00136-8.

(52) Raja, S.; Raghunathan, R.; Yu, X.-Y.; Lee, T.; Chen, J.; Kommalapati, R. R.; Murugesan, K.; Shen, X.; Qingzhong, Y.; Valsaraj, K. T.; Collett, J. L. Fog Chemistry in the Texas–Louisiana Gulf Coast Corridor. *Atmos. Environ.* **2008**, *42* (9), 2048–2061. https://doi.org/https://doi.org/10.1016/j.atmosenv.2007.12.004.

(53) George, K. M.; Ruthenburg, T. C.; Smith, J.; Yu, L.; Zhang, Q.; Anastasio, C.; Dillner, A. M. FT-IR Quantification of the Carbonyl Functional Group in Aqueous-Phase Secondary Organic Aerosol from Phenols. *Atmos. Environ.* **2015**, *100*, 230–237. https://doi.org/10.1016/j.atmosenv.2014.11.011.

(54) Ge, X.; Shaw, S. L.; Zhang, Q. Toward Understanding Amines and Their Degradation Products from Postcombustion CO2 Capture Processes with Aerosol Mass Spectrometry. *Environ. Sci. Technol.* **2014**, *48* (9), 5066–5075. https://doi.org/10.1021/es4056966.

(55) Lin, P.; Fleming, L. T.; Nizkorodov, S. A.; Laskin, J.; Laskin, A. Comprehensive Molecular Characterization of Atmospheric Brown Carbon by High Resolution Mass Spectrometry with Electrospray and Atmospheric Pressure Photoionization. *Anal. Chem.* **2018**, *90* (21), 12493–12502. https://doi.org/10.1021/acs.analchem.8b02177.

(56) Aiken, A. C.; DeCarlo, P. F.; Kroll, J. H.; Worsnop, D. R.; Huffman, J. A.; Docherty, K.

S.; Ulbrich, I. M.; Mohr, C.; Kimmel, J. R.; Sueper, D.; Sun, Y.; Zhang, Q.; Trimborn, A.; Northway, M.; Ziemann, P. J.; Canagaratna, M. R.; Onasch, T. B.; Alfarra, M. R.; Prevot, A. S. H.; Dommen, J.; Duplissy, J.; Metzger, A.; Baltensperger, U.; Jimenez, J. L. O/C and OM/OC Ratios of Primary, Secondary, and Ambient Organic Aerosols with High-Resolution Time-of-Flight Aerosol Mass Spectrometry. *Environ. Sci. Technol.* **2008**, *42* (12), 4478–4485. https://doi.org/10.1021/es703009q.

(57) Kroll, J. H.; Donahue, N. M.; Jimenez, J. L.; Kessler, S. H.; Canagaratna, M. R.; Wilson, K. R.; Altieri, K. E.; Mazzoleni, L. R.; Wozniak, A. S.; Bluhm, H.; Mysak, E. R.; Smith, J. D.; Kolb, C. E.; Worsnop, D. R. Carbon Oxidation State as a Metric for Describing the Chemistry of Atmospheric Organic Aerosol. *Nat Chem* **2011**, *3* (2), 133–139. https://doi.org/10.1038/nchem.948.

(58) Yee, L. D.; Kautzman, K. E.; Loza, C. L.; Schilling, K. A.; Coggon, M. M.; Chhabra, P. S.; Chan, M. N.; Chan, A. W. H.; Hersey, S. P.; Crounse, J. D.; Wennberg, P. O.; Flagan, R. C.; Seinfeld, J. H. Secondary Organic Aerosol Formation from Biomass Burning Intermediates: Phenol and Methoxyphenols. *Atmos. Chem. Phys.* **2013**, *13* (16), 8019–8043. https://doi.org/10.5194/acp-13-8019-2013.

(59) Ulbrich, I. M.; Canagaratna, M. R.; Zhang, Q.; Worsnop, D. R.; Jimenez, J. L. Interpretation of Organic Components from Positive Matrix Factorization of Aerosol Mass Spectrometric Data. *Atmos. Chem. Phys.* **2009**, *9* (9), 2891–2918. https://doi.org/10.5194/acp-9-2891-2009.

(60) Zhang, Q.; Jimenez, J. L.; Canagaratna, M. R.; Ulbrich, I. M.; Ng, N. L.; Worsnop, D. R.; Sun, Y. Understanding Atmospheric Organic Aerosols via Factor Analysis of Aerosol Mass Spectrometry: A Review. *Anal. Bioanal. Chem.* **2011**, *401* (10), 3045–3067. https://doi.org/10.1007/s00216-011-5355-y.

(61) Pluskal, T.; Castillo, S.; Villar-Briones, A.; Orešič, M. MZmine 2: Modular Framework for Processing, Visualizing, and Analyzing Mass Spectrometry-Based Molecular Profile Data. *BMC Bioinformatics* **2010**, *11* (1), 395. https://doi.org/10.1186/1471-2105-11-395.

(62) Roach, P. J.; Laskin, J.; Laskin, A. Higher-Order Mass Defect Analysis for Mass Spectra of Complex Organic Mixtures. *Anal. Chem.* **2011**, *83* (12), 4924–4929. https://doi.org/10.1021/ac200654j.

(63) Pillar, E. A.; Camm, R. C.; Guzman, M. I. Catechol Oxidation by Ozone and Hydroxyl Radicals at the Air–Water Interface. *Environ. Sci. Technol.* **2014**, *48* (24), 14352–14360. https://doi.org/10.1021/es504094x.

(64) Chen, Y.; Li, N.; Li, X.; Tao, Y.; Luo, S.; Zhao, Z.; Ma, S.; Huang, H.; Chen, Y.; Ye, Z.; Ge, X. Secondary Organic Aerosol Formation from 3C∗-Initiated Oxidation of 4-Ethylguaiacol in Atmospheric Aqueous-Phase. *Sci. Total Environ.* **2020**, *723*, 137953. https://doi.org/https://doi.org/10.1016/j.scitotenv.2020.137953.

(65) Heald, C. L.; Kroll, J. H.; Jimenez, J. L.; Docherty, K. S.; DeCarlo, P. F.; Aiken, A. C.; Chen, Q.; Martin, S. T.; Farmer, D. K.; Artaxo, P. A Simplified Description of the Evolution of Organic Aerosol Composition in the Atmosphere. *Geophys. Res. Lett.* **2010**, *37* (8), L08803. https://doi.org/10.1029/2010GL042737.

(66) O'Neill, P.; Steenken, S.; van der Linde, H.; Schulte-Frohlinde, D. Reaction of OH

Radicals with Nitrophenols in Aqueous Solution. *Radiat. Phys. Chem.* **1978**, *12* (1), 13–17. https://doi.org/https://doi.org/10.1016/0146-5724(78)90070-5.

(67) Lin, P.; Liu, J.; Shilling, J. E.; Kathmann, S. M.; Laskin, J.; Laskin, A. Molecular Characterization of Brown Carbon (BrC) Chromophores in Secondary Organic Aerosol Generated from Photo-Oxidation of Toluene. *Phys. Chem. Chem. Phys.* **2015**, *17* (36), 23312–23325. https://doi.org/10.1039/C5CP02563J.

(68) Lin, P.; Aiona, P. K.; Li, Y.; Shiraiwa, M.; Laskin, J.; Nizkorodov, S. A.; Laskin, A. Molecular Characterization of Brown Carbon in Biomass Burning Aerosol Particles. *Environ. Sci. Technol.* **2016**, *50* (21), 11815–11824. https://doi.org/10.1021/acs.est.6b03024.

(69) Mazzoleni, L. R.; Saranjampour, P.; Dalbec, M. M.; Samburova, V.; Hallar, A. G.; Zielinska, B.; Lowenthal, D. H.; Kohl, S. Identification of Water-Soluble Organic Carbon in Non-Urban Aerosols Using Ultrahigh-Resolution FT-ICR Mass Spectrometry: Organic Anions. *Environ. Chem.* **2012**, *9* (3), 285–297.

(70) Kourtchev, I.; Fuller, S. J.; Giorio, C.; Healy, R. M.; Wilson, E.; O'Connor, I.; Wenger, J. C.; McLeod, M.; Aalto, J.; Ruuskanen, T. M.; Maenhaut, W.; Jones, R.; Venables, D. S.; Sodeau, J. R.; Kulmala, M.; Kalberer, M. Molecular Composition of Biogenic Secondary Organic Aerosols Using Ultrahigh-Resolution Mass Spectrometry: Comparing Laboratory and Field Studies. *Atmos. Chem. Phys.* **2014**, *14* (4), 2155–2167. https://doi.org/10.5194/acp-14-2155-2014.

(71) Hecobian, A.; Zhang, X.; Zheng, M.; Frank, N.; Edgerton, E. S.; Weber, R. J. Water-Soluble Organic Aerosol Material and the Light-Absorption Characteristics of Aqueous Extracts Measured over the Southeastern United States. *Atmos. Chem. Phys.* **2010**, *10* (13), 5965–5977. https://doi.org/10.5194/acp-10-5965-2010.

(72) Kirchstetter, T. W.; Thatcher, T. L. Contribution of Organic Carbon to Wood Smoke Particulate Matter Absorption of Solar Radiation. *Atmos. Chem. Phys.* **2012**, *12* (14), 6067–6072. https://doi.org/10.5194/acp-12-6067-2012.

(73) Mang, S. A.; Henricksen, D. K.; Bateman, A. P.; Andersen, M. P. S.; Blake, D. R.; Nizkorodov, S. A. Contribution of Carbonyl Photochemistry to Aging of Atmospheric Secondary Organic Aerosol. *J. Phys. Chem. A* **2008**, *112* (36), 8337–8344. https://doi.org/10.1021/jp804376c.

(74) Kobayashi, S.; Higashimura, H. Oxidative Polymerization of Phenols Revisited. *Prog. Polym. Sci.* **2003**, *28* (6), 1015–1048. https://doi.org/10.1016/S0079-6700(03)00014-5.

Supporting Information:

Photosensitized Reactions of a Phenolic Carbonyl from Wood Combustion in the Aqueous Phase – Chemical Evolution and Light Absorption Properties of AqSOA

Wenqing Jiang[1,2], Maria V Misovich[3], Anusha P.S. Hettiyadura[3], Alexander Laskin[3,4], Alexander S. McFall[2,5], Cort Anastasio[2,5], Qi Zhang[1,2]*

[1]Department of Environmental Toxicology, University of California, Davis, CA

[2]Agricultural and Environmental Chemistry Graduate Group, University of California, Davis, CA

[3]Department of Chemistry, Purdue University, West Lafayette, IN

[4]Department of Earth, Atmospheric and Planetary Sciences, Purdue University, West Lafayette, IN

[5]Department of Land, Air, and Water Resources, University of California, Davis, CA

*Corresponding author: Qi Zhang

Email: dkwzhang@ucdavis.edu

Phone: 530-752-5779

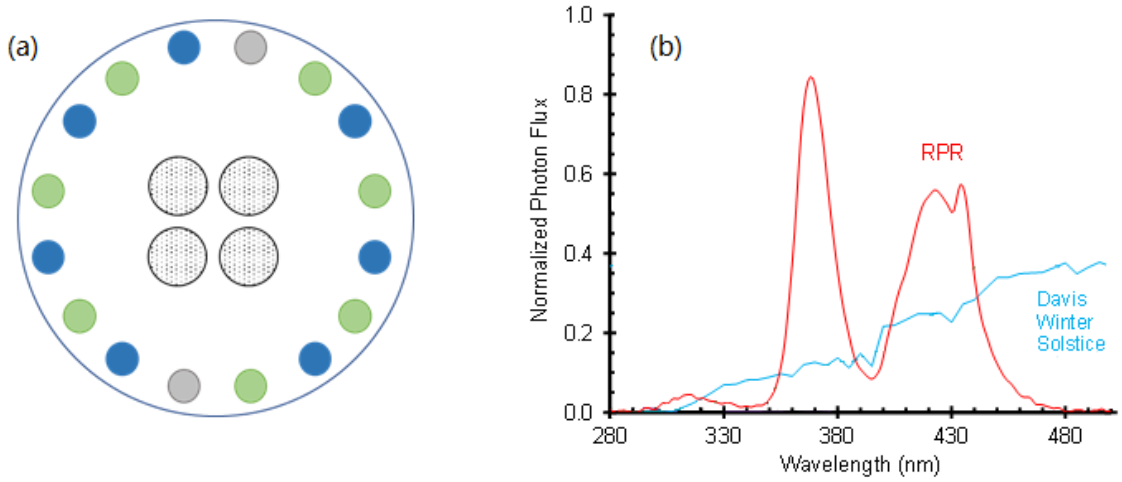

Figure S1. (a) Top-down diagram of the bulb and samples in the RPR-200 photoreactor. The four central, dotted circles are the Pyrex tubes containing samples for illumination, and the peripheral grey, green, and blue circles are RPR-3000, RPR-3500, and RPR-4190 bulbs, respectively. The fan and stir plates are located directly beneath the sample tubes, and each illuminated sample tube contains a stir bar; (b) Normalized distribution of the photon flux inside the RPR-200 photoreactor, and for comparison, the actinic flux in Davis, CA at winter solstice.1 Photon fluxes are normalized such that the area under each curve between 280 and 500 nm is equal.

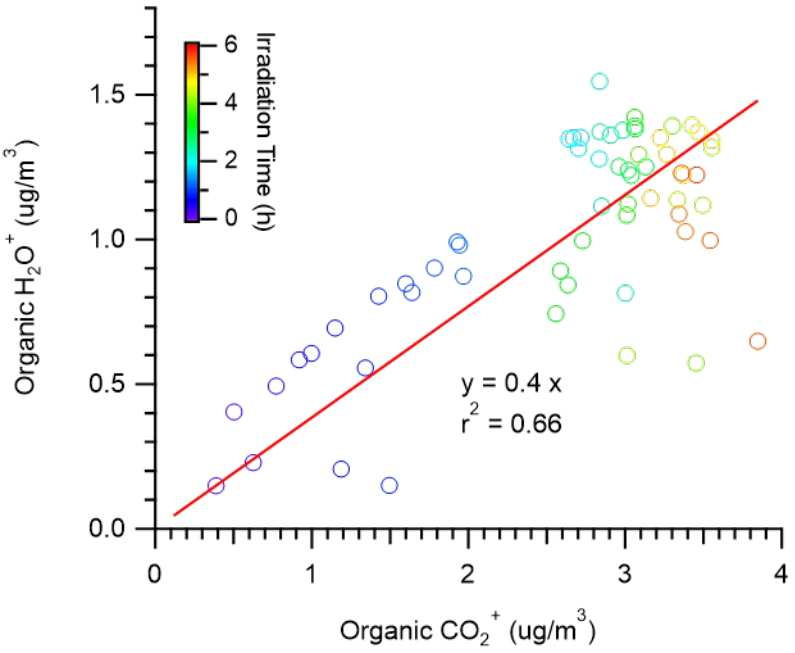

Figure S2. Correlation between the organic H_2O^+ signal (= total H_2O^+ signal - sulfate H_2O^+ signal) and the CO_2^+ signal measured in the AMS spectra of the aqSOA samples

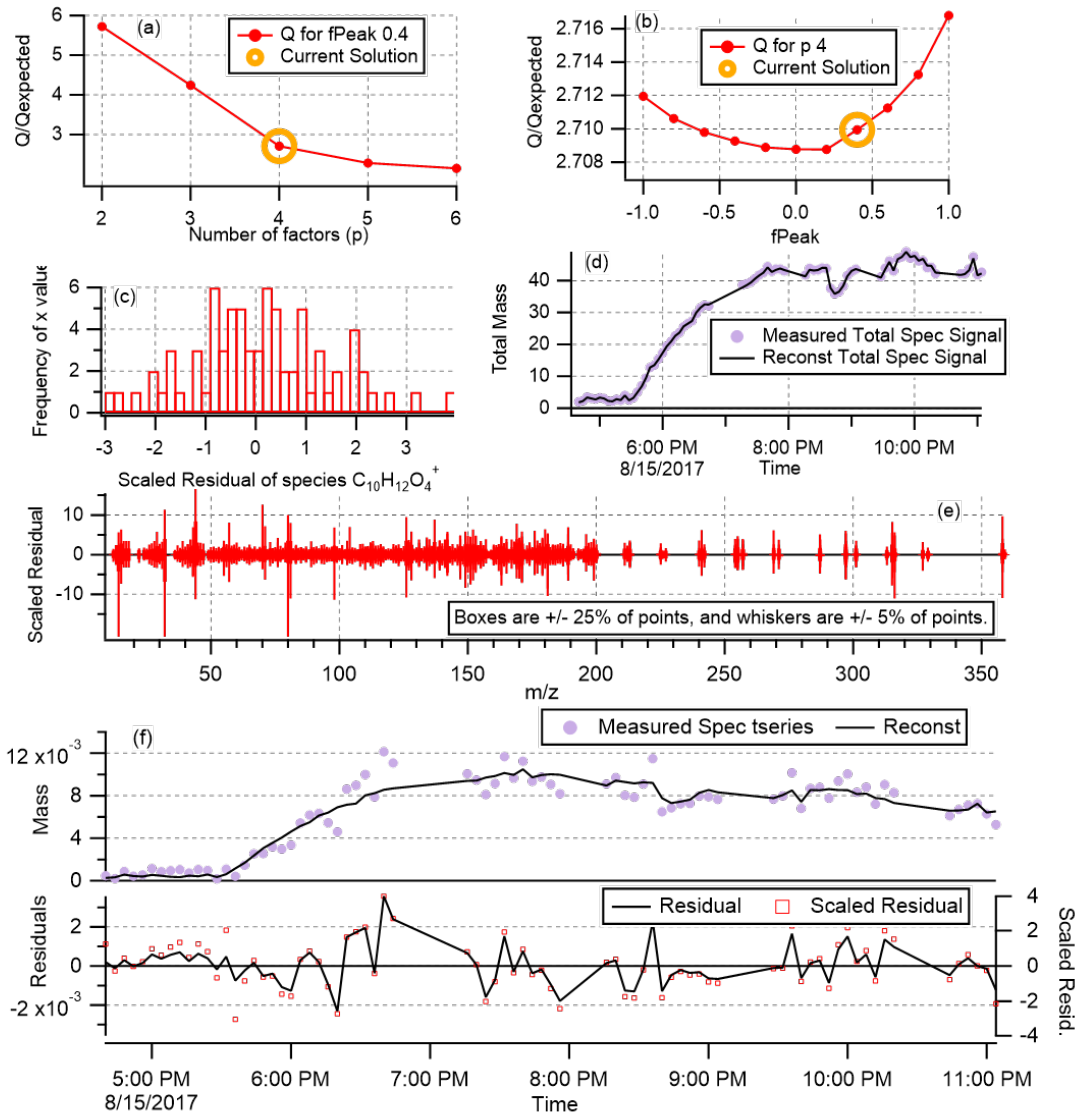

Figure S3. Summary of diagnostic plots for the four-factor solution for PMF analysis: (a) Q/Qexp as a function of number of factors selected for PMF modeling; (b) Q/Qexp as a function of fPeak; (c) Histogram of scaled residuals for species $C_{10}H_{12}O_4^+$; (d) Reconstructed and measured total species signal for all species; (e) box and whisker plot showing the distributions of scaled residuals for each m/z; and (f) Reconstructed and measured signals and residuals for species $C_{10}H_{12}O_4^+$

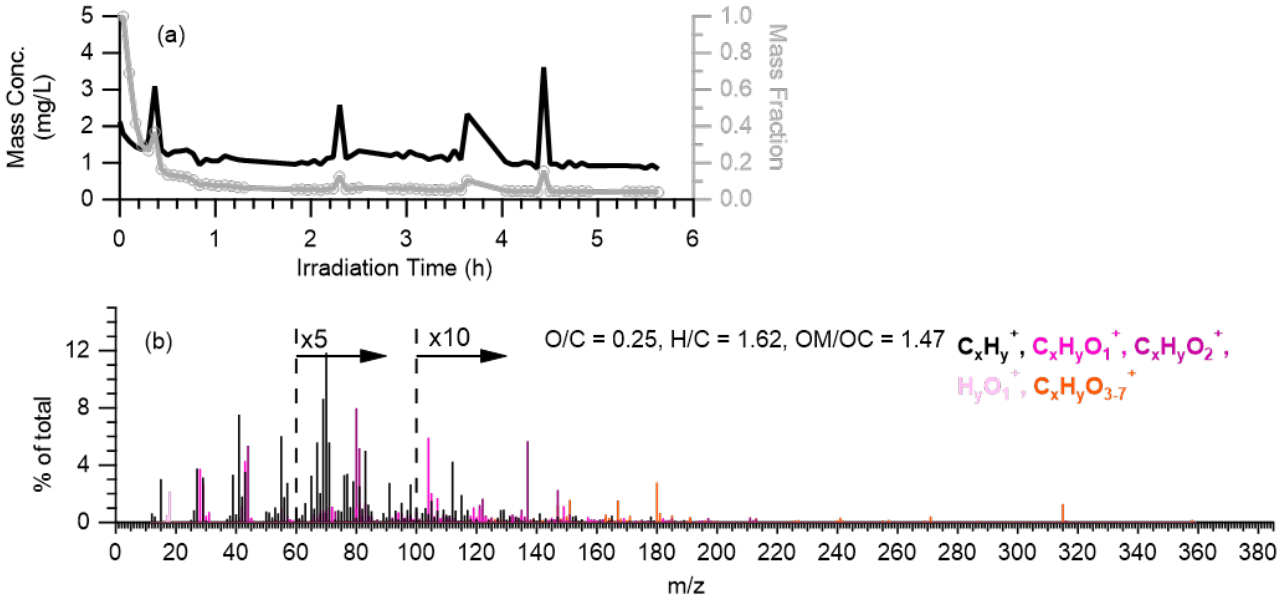

Figure S4. (a) Mass concentration and fraction time series and (b) MS profile of the background factor obtained from PMF analysis

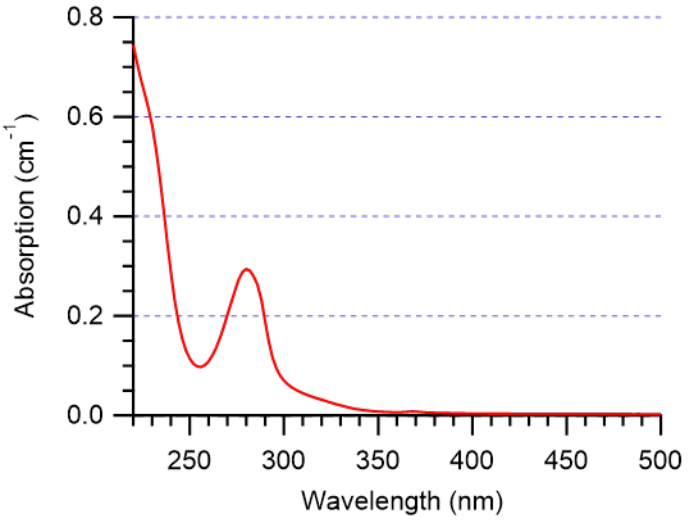

Figure S5. UV-vis absorption spectrum of 100 μM of GA standard

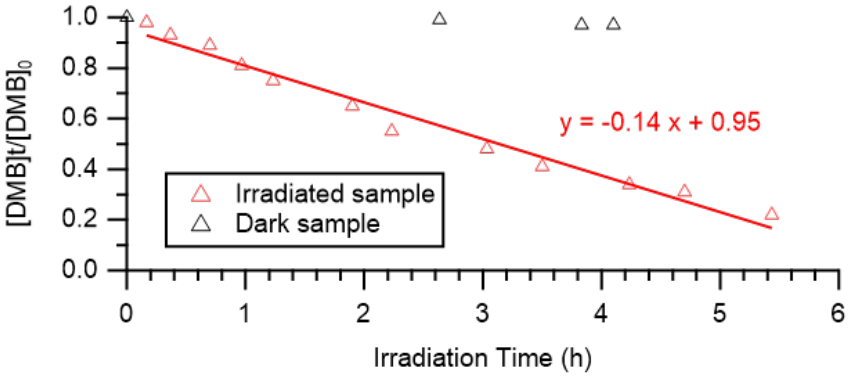

Figure S6. Loss of 3,4-DMB in the reaction solution. The irradiation time for each sample was calculated as the mean of the sampling start time and end time.

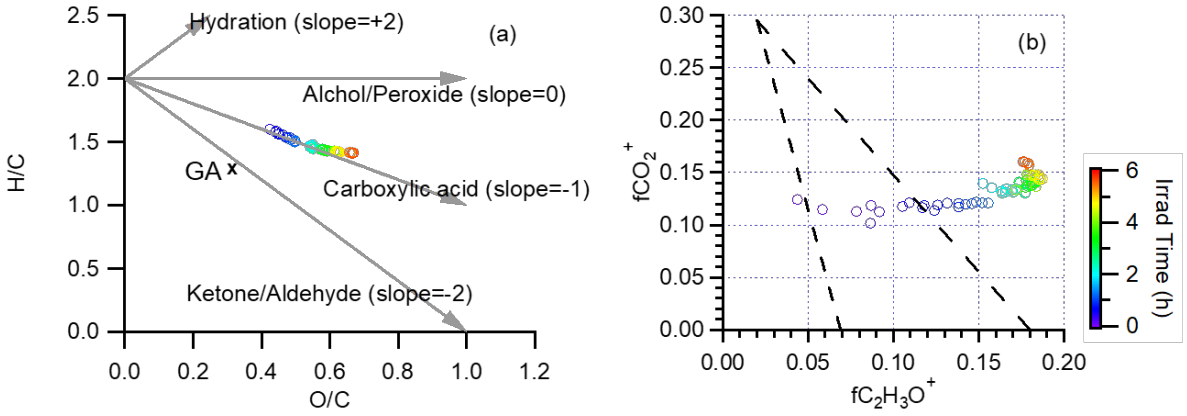

Figure S7. (a) Van Krevelen Diagram and (b) AMS measured mass fraction of $C_2H_3O^+$ and CO_2^+ of aqSOA products formed in the photoreaction experiment of GA with $^3C^*$

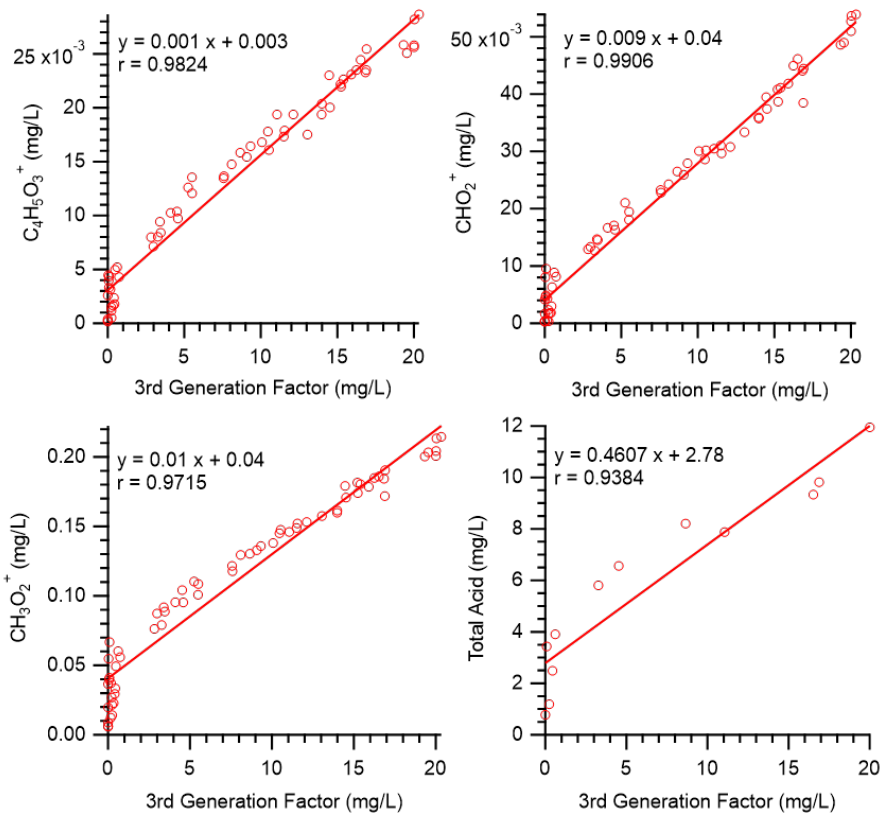

62

63 Figure S8. Correlation between the time series of selected ions and the 3rd generation products factor
64 from PMF analysis.

65

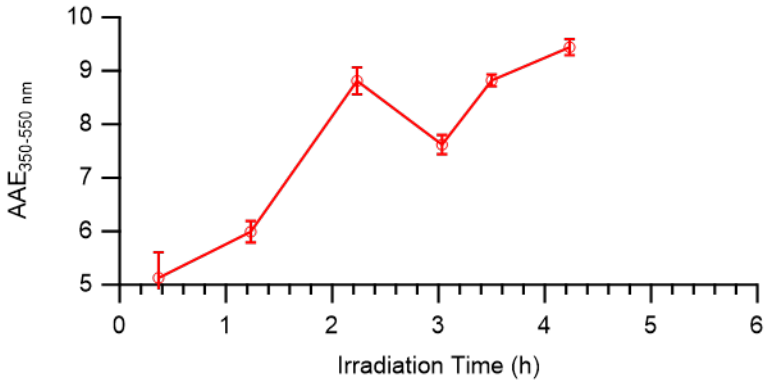

Figure S9. Time series of the Absorption Angstrom Exponents (AAE) for the illuminated reaction solution. Error bars represent ±1 standard error (SE) calculated by propagating the uncertainties.

Scheme S1. Possible products produced during photooxidation of GA through oligomerization, hydroxylation, and demethoxylation.